Annals of Operations Research
https://doi.org/10.1007/s10479-025-06759-6

ORIGINAL RESEARCH

Cooperation against invasions: multi-agent control of alien species in connected landscapes

Andrea Caravaggio[1] · **Andrea Di Liddo**[2] · **Angela Martiradonna**[2]

Received: 30 April 2025 / Accepted: 8 July 2025

Abstract
Invasive alien species (IAS) increasingly threaten biodiversity, ecosystem services, and economic sustainability, particularly in fragmented landscapes where management responsibilities are decentralized. The spread of IAS is not confined within administrative borders but it follows ecological connectivity, making isolated local interventions often ineffective. This work presents a dynamic game-theoretic framework for modeling the strategic management of IAS across a network of heterogeneous areas linked by spatial diffusion. Each agent, responsible for local control of the invasion, faces a trade-off between reducing ecological damages and sustaining the economic costs of intervention. The analysis explores how the interaction between spatial structure, ecological features, and decentralized decision-making shapes outcomes under non-cooperative, coalition-based, and fully cooperative strategies. To support the cooperative behavior, fair cost-allocation mechanisms are proposed based on Nash bargaining and the Myerson value, explicitly accounting for spatial externalities. Numerical experiments on a synthetic three-node network illustrate how cooperation can substantially reduce invasion spread and management costs, while strategic defection may exacerbate both ecological and economic losses. The main findings of the analysis underline the vulnerabilities of fragmented management and the need for institutional arrangements to promote adaptive, equitable, and spatially informed strategies for IAS control.

Keywords Invasive alien species · Differential games on networks · Multi-agent systems · Nash bargaining · Myerson value

✉ Angela Martiradonna
angela.martiradonna@unifg.it

Andrea Caravaggio
andrea.caravaggio@unisi.it

Andrea Di Liddo
andrea.diliddo@unifg.it

[1] Department of Economics and Statistics, University of Siena, Piazza San Francesco 7, 53100 Siena, Italy

[2] Department of Economics, University of Foggia, Via Romolo Caggese 1, 71121 Foggia, Italy

Published online: 01 August 2025

Mathematic Subject Classification 34A34 · 49L12 · 91A25 · 91B32 · 91B76

JEL Classification C61 · C73 · Q57

1 Introduction

Invasive alien species (IAS) pose an escalating global threat, significantly impacting ecological integrity, economic sustainability, and public health as they rapidly colonize and spread in non-native environments (Warziniack et al., 2021). The intensification of global trade, climate change, increased human mobility, and expansive transportation networks have accelerated the proliferation of IAS, presenting complex challenges to management and requiring advanced, integrated strategies (Ahmed et al., 2022; Hauser & McCarthy, 2009). Economically, IAS cause extensive damages across vital sectors, including agriculture, forestry, fisheries, and infrastructure, with estimated annual costs surpassing €12 billion in Europe and over $1.4 trillion globally (Pimentel et al., 2001; Scalera et al., 2012).

IAS impacts extend beyond direct economic losses, significantly disrupting essential ecosystem services such as carbon storage, water purification, and biodiversity conservation. These disruptions amplify public health risks by facilitating the spread of diseases, thus intensifying long-term ecological and socio-economic consequences (Ahmed et al., 2022). In Italy, notable examples include *Ailanthus altissima*, a fast-growing invasive tree that disrupts both urban and rural ecosystems through vigorous root suckering and wind-dispersed seeds, requiring targeted and repeated management interventions supported by spatial analyses and dynamical modeling (Baker et al., 2023). Similarly, the blue crab (*Callinectes sapidus*) threatens marine biodiversity and the economic sustainability of fisheries along Italian coastlines, particularly within ecologically vulnerable areas such as Puglia's Lesina lagoon (Mancinelli et al., 2024), as well as throughout the Mediterranean.

Traditional IAS management practices, such as chemical and physical eradication methods, often prove insufficient due to their high costs, limited effectiveness, and potential environmental harm (Brown & Daigneault, 2014). This situation necessitates strategic decision-making approaches that integrate ecological dynamics, economic considerations, and socio-political contexts (Epanchin-Niell & Wilen, 2012; Fernandez, 2011). Moreover, as IAS typically spread across administrative boundaries, effective management strategies must consider the interdependent nature of control efforts and the need for coordinated actions between multiple stakeholders and jurisdictions (Cobourn et al., 2019; Büyüktahtakin et al., 2011).

Current research underscores the value of optimal control models in IAS management, particularly emphasizing the strategic allocation of resources across temporal and spatial scales to optimize ecological and economic outcomes. These models account for handling times, budget constraints, and regional differences in species dynamics (Baker et al., 2018, 2019; Marangi et al., 2020). Additionally, the recent study provided in Di Liddo and Martiradonna (2025) further demonstrated the utility of optimal control frameworks, examining trade-offs between immediate costs and long-term ecological outcomes in both density-dependent and density-independent scenarios.

The challenge of invasive species management is further exacerbated by the spatial fragmentation of habitats and the ecological connectivity that facilitates species movement

across adjacent or connected areas. In many cases, administrative boundaries do not align with ecological ones, and species can easily spread across landscapes through natural corridors, human-mediated transport, or passive diffusion. This spatial interdependence creates a mismatch between local responsibilities and transboundary ecological processes, often leading to inefficiencies or duplication of control efforts. Effective management thus requires not only localized interventions but also a spatially coordinated response that accounts for the dynamics of invasion across interconnected regions (With, 2002).

Differential game theory provides an effective analytical framework for modeling such strategic interactions involving multiple decision-makers whose actions influence both their outcomes and those of others over time (Lampert et al., 2014; Siriwardena et al., 2018). By explicitly accounting for temporal dynamics, spatial diffusion processes, and strategic behaviors, differential games facilitate the identification of optimal management strategies, revealing potential cooperative and non-cooperative scenarios (Mehta et al., 2007; Eppinga et al., 2021). These methods can identify conditions under which stakeholders benefit from collaboration, providing insights into incentive mechanisms and bargaining strategies that enhance the effectiveness and efficiency of IAS management.

In this paper, we present a spatial and multi-agent extension of the optimal control framework introduced in Di Liddo and Martiradonna (2025). While the original model focused on a single, homogeneous area managed by a centralized decision-maker, here we generalize the framework to a network of interconnected regions, where each node is governed by an independent agent implementing local control strategies and spatial interactions are explicitly modeled. Specifically, we model strategic interactions through a coalition-based framework that allows for various degrees of cooperation among agents. These strategic settings are formalized as differential games that capture the incentives and interactions among agents over time. The resulting control problems are solved using the Pontryagin Maximum Principle (Pontryagin, 2018), while the Hamilton–Jacobi–Bellman equations (Bertsekas, 2012) are introduced as a theoretical reference for characterizing optimal feedback strategies. In our analysis, we compare two benchmark strategic paradigms: the fully non-cooperative one, where agents act independently, and the fully cooperative one, where all agents coordinate to minimize the total system cost. The coalition-based structure also allows us to characterize intermediate configurations, in which subsets of agents cooperate while others act independently. In the cooperative setting, we further address the problem of cost allocation by applying two game theoretic mechanisms: the Nash bargaining solution, which distributes cooperative gains based on negotiated benefits (Nash, 1950), and the Myerson value, which accounts for each agent's marginal contribution within a network of potential coalitions (Myerson, 1977).

To illustrate the applicability of the model, we conduct numerical simulations on a synthetic three-node network representing a fragmented landscape. We perform a sensitivity analysis on spatial connectivity, control costs, and habitat suitability to assess their impact on the benefits of cooperation. Finally, we examine a heterogeneous scenario with realistic areas and evaluate cost allocation under different coalition structures using the Nash bargaining solution and the Myerson value.

The remainder of the paper is structured as follows. Section 2 presents the core components of the model, with particular emphasis on the spatial diffusion mechanism, population dynamics, and the cost structure faced by each agent in the network. Section 3 analyzes the non-cooperative game setting. Section 4 extends the framework to strategic interac-

tions among agents, including both partial coalitions and full cooperation. Section 5 introduces two alternative cost-allocation mechanisms within the cooperative setting: the Nash bargaining solution and the Myerson value. Section 6 reports numerical experiments that highlight the effects of heterogeneity on control efforts, cost allocation, and invasive species dynamics across the network. Finally, Section 7 concludes the paper.

2 Population dynamics and control objectives

We consider a network of $N \geq 2$ areas where an invasive alien species spreads or could potentially spread. These areas may represent local zones, protected sites, or even different countries. Each area $i = 1, \ldots, N$ is managed by a local agent (or decision-maker), such as a park manager, local authority, private landowner, or a stakeholder operating an agricultural or productive activity, who is responsible for implementing time-dependent strategies to control the local population of the invasive species in area i.

2.1 Local dynamics

The local dynamics in each area i are described by the following differential equation:

$$\dot{x}_i(t) = f_i(x_i(t)) - u_i(t)\, g_i(x_i(t)), \quad x_i(0) = x_i^0. \tag{1}$$

Here, $x_i(t)$ denotes the population size of the invasive species in area i at time t, and $x_i^0 \geq 0$ represents the initial population level in that area. The term $f_i(x_i)$ models the intrinsic growth of the species in area i. To limit the invasion, each local agent implements a control action through a time-dependent effort $u_i(t) \geq 0$, which may involve mechanical, chemical, or biological interventions. The effectiveness of such control depends on the current population size and is represented by a function $g_i(x_i)$.

As in Di Liddo and Martiradonna (2025), we make the following assumptions on the local growth and control effectiveness functions $f_i(x_i)$ and $g_i(x_i)$, for all $i = 1, \ldots, N$:

(A1) The functions $f_i(x_i)$ and $g_i(x_i)$ are non-negative, continuous, and continuously differentiable.

(A2) The functions satisfy the following growth condition:

$$|f_i(x_i) - g_i(x_i)\, u_i| \leq C_i(1 + |x_i| + |u_i|), \quad \text{for some constants } C_i > 0.$$

(A3) $f_i(0) = g_i(0) = 0$, meaning that when the population size is zero, there is neither intrinsic growth nor control effect.

The intrinsic growth function $f_i(x_i)$ is typically modeled using either an exponential or a logistic form. In the exponential case, population grows proportionally to its current size, following $f_i(x_i) = r_i\, x_i$, whereas the logistic formulation accounts for saturation effects and is given by $f_i(x_i) = r_i\, x_i \left(1 - \frac{x_i}{K_i}\right)$. Here, $r_i > 0$ denotes the intrinsic growth rate, and $K_i > 0$ is the carrying capacity in area i.

The function $g_i(x_i)$, representing the effectiveness of control efforts, captures how removal rates vary with population density. Inspired by Holling's functional responses

(Holling, 1959), it can take different forms depending on the ecological assumptions. A linear response is expressed as $g_i(x_i) = \mu_i\, x_i$, where removal increases proportionally with abundance (Type I). A more realistic saturating behavior is captured by the Type II function $g_i(x_i) = \frac{\mu_i\, x_i}{1+\tau_i\, \mu_i\, x_i}$, which reflects diminishing returns at higher densities. Finally, the Type III response, given by $g_i(x_i) = \frac{\mu_i\, x_i^2}{1+\tau_i\, \mu_i\, x_i^2}$, introduces low efficiency at low densities and a sigmoidal shape characteristic of threshold-driven control. In all cases, $\mu_i > 0$ represents the maximum per-unit effort removal rate, and $\tau_i > 0$ regulates the onset of saturation.

Additionally, size-independent scenarios can be modeled by assuming a constant control function of the form $g_i(x_i) = \mu_i$, which represents situations where the effectiveness of control remains uniform regardless of the current population size. This may arise, for instance, when interventions are applied with fixed effort, or when chemical treatments produce the same effect independently of species abundance. However, this specification violates the structural assumptions of the model and therefore requires a more careful treatment, as discussed in Di Liddo and Martiradonna (2025).

In all these formulations, the parameters r_i, K_i, μ_i, τ_i can be influenced by ecological conditions such as resource availability, climate, or habitat type, as well as by the efficiency of the control strategies, and may either vary across areas or be assumed constant depending on the application context.

2.2 Spatial diffusion structure

The model in Di Liddo and Martiradonna (2025) is now extended to incorporate the spatial diffusion of the species across areas. The invasive species can spread throughout the network, moving from one area to another as a result of local differences in population size. In this framework, the *network* is understood as a set of N interconnected areas, where each pair of areas may or may not be directly linked through potential pathways for movement. The diffusion intensity between two areas is modeled through non-negative coefficients that may depend on their ecological or geographical distance. In general, areas that are closer or more strongly connected allow for higher movement, while distant or poorly connected areas experience weaker interactions. Throughout this paper, we assume that the network is connected, meaning that it is possible to reach any area from any other through a sequence of direct connections.

The interaction among areas is modeled through *diffusion terms* of the form $\sigma_{ij}(x_j - x_i)$, which describe the net flow of individuals between area j and area i. The direction of this flow depends on the sign of the population difference: the species move from the more densely populated area to the less populated one. The coefficient $\sigma_{ij} \geq 0$ quantifies the intensity of the connection between areas i and j, and we assume symmetry, that is $\sigma_{ij} = \sigma_{ji}$. This implies that the potential for movement is reciprocal, and it is essential for guaranteeing *mass conservation* across the network in the absence of local growth or control. The coefficients σ_{ij} may be zero to reflect physical, ecological, or anthropogenic barriers, such as mountains, habitat fragmentation, infrastructure, or containment policies. These zero entries define the absence of direct connections between specific areas. A similar diffusion mechanism was studied in the two-patch case in Bischi et al. (2009), where the dynamics of fish stocks under different harvesting regimes were analyzed in the context of a marine protected area. A recent contribution that formalizes diffusion and externalities on

network structures is Fabbri et al. (2024), where growth dynamics are studied in presence of spatial interactions and network topology.

To illustrate how the structure of the diffusion network influences the system's connectivity and potential for species spread, Fig. 1 shows two representative configurations involving four areas. On the left, all pairs of areas are directly connected by symmetric diffusion terms, resulting in a fully connected network. On the right, only external links between adjacent areas are active, while the diagonal connections between areas 1–3 and 2–4 are inactive ($\sigma_{13} = \sigma_{31} = \sigma_{24} = \sigma_{42} = 0$). Despite these missing links, the network remains connected: there still exists a path between any pair of nodes.

The overall structure of the diffusion network is encoded in the matrix $S \in \mathbb{R}^{N\times N}$, whose entries are defined as:

$$S_{ij} = \begin{cases} \sigma_{ij}, & \text{if } i \neq j, \\ -\sum_{k\neq i} \sigma_{ik}, & \text{if } i = j. \end{cases} \tag{2}$$

By construction, S is a *Laplacian matrix* associated with the undirected weighted network with diffusion coefficients σ_{ij}, as in the classical formulation of spectral graph theory (Chung, 1997).

The main properties of the matrix S are summarized in the proposition below. The first four follow directly from its definition, while property *(v)* is a classical result in spectral graph theory, stating that the only steady state (up to scaling) of the pure diffusion dynamics corresponds to a spatially uniform distribution (Chung, 1997).

Proposition 1 *The following properties hold for the matrix S:*

(i) S is symmetric;

(ii) S is positive semidefinite: $\mathrm{x}^\top S\mathrm{x} = \frac{1}{2}\sum_{i,j=1}^{N} \sigma_{ij}(x_i - x_j)^2 \geq 0$, for all $\mathrm{x} \in \mathbb{R}^N$;

(iii) S satisfies the row-sum condition: $\sum_{j=1}^{N} S_{ij} = 0$ for all $i = 1, \ldots, N$. This ensures *mass conservation* in the absence of local growth and control;

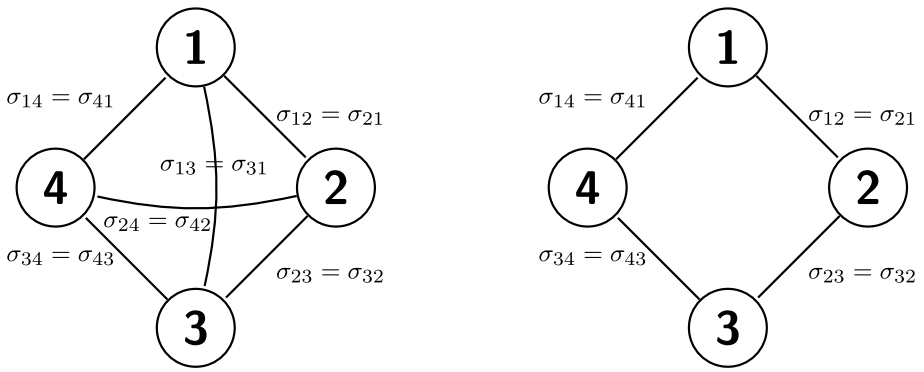

Fig. 1 Two examples of diffusion networks with four areas. *Left:* fully connected network, where all pairs of areas are directly linked by symmetric diffusion rates ($\sigma_{ij} = \sigma_{ji} > 0$). *Right:* connected configuration with only external adjacent links, where the diagonal connections are inactive ($\sigma_{13} = \sigma_{31} = \sigma_{24} = \sigma_{42} = 0$)

(iv) S is singular: zero is always an eigenvalue, and the associated eigenvector is the constant vector $1 = (1, \ldots, 1)^\top$, representing a uniform population distribution;
(v) If the network is connected, then the zero eigenvalue is simple.

2.3 Spatially structured dynamics

The full diffusion contribution to the dynamics of area i is given by the term $\sum_{j=1}^{N} \sigma_{ij}(x_j - x_i)$, which aggregates the net effect of all pairwise interactions and models the total net inflow (or outflow) resulting from population differences between i and the areas to which it is connected. Starting from the local dynamics in (1), we add the diffusion term to obtain the following spatially structured system:

$$\dot{x}_i = f_i(x_i) + \sum_{j=1}^{N} \sigma_{ij}(x_j - x_i) - u_i(t)\, g_i(x_i), \quad x_i(0) = x_i^0, \quad i = 1, \ldots, N. \tag{3}$$

The system can be compactly written in vector form as:

$$\dot{\mathrm{x}}(t) = \mathrm{f}(\mathrm{x}) + S\,\mathrm{x} - G(\mathrm{x})\,\mathrm{u}(t), \quad \mathrm{x}(0) = \mathrm{x}_0, \tag{4}$$

where:

- $\mathrm{x}(t) = (x_1(t), \ldots, x_N(t))^\top \in \mathbb{R}^N$ is the state vector representing the population size in each area;
- $\mathrm{x}_0 = (x_1^0, \ldots, x_N^0)^\top \in \mathbb{R}^N$ is the initial state vector;
- $\mathrm{u}(t) = (u_1(t), \ldots, u_N(t))^\top \in \mathbb{R}^N$ is the vector of local control efforts;
- $\mathrm{f}(\mathrm{x}) = (f_1(x_1), \ldots, f_N(x_N))^\top \in \mathbb{R}^N$ is the vector of local growth terms;
- $G(\mathrm{x}) \in \mathbb{R}^{N \times N}$ is a diagonal matrix encoding the effectiveness of the control in each area:

$$G(\mathrm{x}) = \begin{pmatrix} g_1(x_1) & 0 & \cdots & 0 \\ 0 & g_2(x_2) & \cdots & 0 \\ \vdots & \vdots & \ddots & \vdots \\ 0 & 0 & \cdots & g_N(x_N) \end{pmatrix}.$$

The following proposition states the existence, uniqueness, and positivity of solutions. A detailed proof is provided in Appendix A.

Proposition 2 *Under Assumptions (A1)–(A2), system (4) has a unique global solution* $\mathrm{x}(t)$ *on the interval* $[0, T]$ *for any initial vector* x_0 *and any measurable control* $\mathrm{u}(t)$. *The solution depends continuously on* x_0 *and* u. *Moreover, when also Assumption (A3) holds and* $x_i^0 \geq 0$ *for all* $i = 1, \ldots, N$, *then the solution satisfies* $x_i(t) \geq 0$ *for all* $t \in [0, T]$ *and all* $i = 1, \ldots, N$.

The total population dynamics Let $X(t) := 1^\top x(t) = \sum_{i=1}^{N} x_i(t)$ denote the total population of the invasive species across all areas at time t, where $1 \in \mathbb{R}^N$ is the vector of ones.

The total population $X(t)$ represents the sum of the abundance of the species in all areas at any given time, providing a global measure of the species' spread within the entire network.

From the vector form of the system, we obtain the total population dynamics by left-multiplying both sides by $1^\top$. Recalling the mass-conservation property of the diffusion term, namely $1^\top S = 0$, we obtain:

$$\dot{X}(t) = 1^\top \dot{\mathrm{x}}(t) = 1^\top \mathrm{f}(\mathrm{x}(t)) - 1^\top G(\mathrm{x}(t))\,\mathrm{u}(t).$$

This expression shows that the total population is affected only by local growth and control, while diffusion merely redistributes the species without altering its total mass. This mass-conserving property enables a clear assessment of the overall impact of control strategies across the entire network.

While the total population dynamics provide a global perspective, management decisions are made locally by individual agents responsible for each area. We now describe the cost functionals that govern these decisions.

2.4 Agent-specific objective functionals

We use the notation $x_i(t;\mathrm{u})$ to denote the population size of the invasive species in area i at time t, under the control profile $\mathrm{u}(t)$. The dependence on the full control vector reflects the fact that the population dynamics are coupled across areas through the diffusion process. Therefore, the control applied by one agent affects not only the state in their own area but also the states in the others, due to the spatial connectivity encoded in the diffusion matrix S. As a consequence, the cost incurred by each agent depends not only on their own control action but is also influenced by the decisions made by the other agents.

The cost functional for agent i includes both direct and indirect costs. The former refer to the expenses directly associated with the control effort, such as labor, equipment, and chemical or mechanical interventions: these are modeled through a quadratic term to account for increasing marginal costs. The latter arise from the ecological and economic damages caused by the invasive species, including losses in agricultural productivity, damage to infrastructure, reductions in biodiversity, and negative effects on tourism and ecosystem services.

Following (Di Liddo & Martiradonna, 2025), the cost functional for agent i is given by:

$$J_i(\mathrm{u}) = e^{-\rho T}\phi_i(x_i(T;\mathrm{u})) + \int_0^T e^{-\rho t}\left[E_i(x_i(t;\mathrm{u})) + \frac{d_i}{2}(u_i(t))^2\right] dt, \tag{5}$$

where:

- $E_i(x_i(t;\mathrm{u}))$ represents the *indirect cost*, reflecting the environmental and economic impact of the invasive species in area i at time t;
- $\frac{d_i}{2}(u_i(t))^2$ represents the *direct cost* of the control effort in area i, modeled as a quadratic function to capture increasing marginal costs. Here, $d_i > 0$ is a positive parameter reflecting the sensitivity of the cost to the control intensity. More specifically, the higher d_i the more expensive the control of the species in the area, conversely the lower d_i the less impact the control activity has on the costs incurred in the area;

- $\phi_i(x_i(T;\mathrm{u}))$ is the *terminal cost*, representing the residual environmental damage at the final time T due to the remaining invasive population in area i;
- $\rho \geq 0$ is the *discount rate*, which reflects the agent's preference for present costs over future ones.

We make the following additional assumptions on the cost functions:

(A4). The functions $E_i(x)$ and $\phi_i(x)$ are non-negative and continuous on $[0, +\infty)$;
(A5). The function $E_i(x)$ satisfies $E_i(0) = 0$, meaning that no cost is incurred in the absence of the invasive species. Moreover, $E_i(x)$ is increasing, reflecting the principle that ecological and economic damages increase with the local population size.

The control functions $u_i(t)$ are required to be non-negative and square integrable over the time interval $[0, T]$. Therefore, the admissible set of controls for all agents is defined as:

$$\mathcal{U} = \left\{ u \in L^2(0,T) : u(t) \geq 0 \text{ a.e. in } [0,T] \right\}.$$

3 Optimal strategies in the non-cooperative game

We now formulate a non-cooperative dynamic game among the N local agents, where each agent $i = 1, \ldots, N$ independently selects a control strategy $u_i \in \mathcal{U}$ with the goal of minimizing its own cost functional J_i, defined in (5). Due to the coupling between areas introduced by the spatial diffusion term in the dynamics (4), each agent's decision affects not only their own state but also the evolution of the entire system. The resulting game can be compactly written as:

$$\min_{u_i \in \mathcal{U}} J_i(\mathrm{u}) \quad \text{for all } i = 1, \ldots, N, \quad \text{subject to the state dynamics (4).} \tag{6}$$

Definition 1 A control profile $\mathrm{u}^* = (u_1^*, \ldots, u_N^*) \in \mathcal{U}^N$ is said to be an *Nash equilibrium* for game (6) if, for each agent $i = 1, \ldots, N$, the control u_i^* solves the following optimal control problem:

$$\min_{u_i \in \mathcal{U}} J_i(u_i, \mathrm{u}^*_{-i}), \quad \text{subject to the state dynamics (4),} \tag{7}$$

where $\mathrm{u}^*_{-i} = (u_1^*, \ldots, u_{i-1}^*, u_{i+1}^*, \ldots, u_N^*)$. The corresponding state trajectory $\mathrm{x}^*(t)$ is the solution of the system (4) under the equilibrium control profile u^*.

Proposition 3 *Let Assumptions (A1)–(A4) hold. Then, there exists an open-loop Nash equilibrium control profile* $\mathrm{u}^* = (u_1^*, \ldots, u_N^*) \in \mathcal{U}^N$ *for game (6) and an associated state trajectory* $\mathrm{x}^*(t)$.

The proof of Proposition 3 follows by applying standard arguments from optimal control theory and is reported in Appendix A for completeness. The construction relies on the con-

vexity of the control set, the continuity of the cost functional, and the well-posedness of the state dynamics.

In our model, optimal strategies can be formulated either in *open-loop* form, where each control function $u_i(t)$ is predetermined and depends only on time, or in *state-feedback* form, where control actions are continuously adjusted according to the current state of the system. These two approaches reflect different levels of information and responsiveness. Feedback strategies provide enhanced flexibility by enabling agents to react dynamically to time-by-time observations of population abundance. This makes them especially appropriate in contexts characterized by high monitoring capacity or short-term decision-making cycles. In contrast, open-loop strategies are typically adopted in ecological control programs where actions are planned ahead of time–such as seasonal eradication efforts, resource-constrained policies, or large-scale interventions–without continuous access to updated state information.

We now derive the necessary conditions that characterize equilibrium strategies in both the *open-loop* and *state-feedback* formulations. In the open-loop setting, we obtain first-order necessary conditions based on Pontryagin's Maximum Principle. In the feedback formulation, optimality is instead characterized by the Hamilton–Jacobi–Bellman (HJB) equation, which provides a necessary condition on the value function associated with each agent. Under suitable regularity assumptions, the HJB framework also yields sufficient conditions for optimality and allows the derivation of optimal feedback policies.

3.1 Open-loop Nash equilibrium

To derive necessary conditions for an open-loop Nash equilibrium, we introduce the matrix of adjoint variables $\Lambda(t) \in \mathbb{R}^{N\times N}$, where each row corresponds to the adjoint vector of a specific agent:

$$\Lambda(t) = \begin{bmatrix} \boldsymbol{\lambda}_1^\top(t) \\ \boldsymbol{\lambda}_2^\top(t) \\ \vdots \\ \boldsymbol{\lambda}_N^\top(t) \end{bmatrix} = \begin{bmatrix} \lambda_{11}(t) & \cdots & \lambda_{1N}(t) \\ \lambda_{21}(t) & \cdots & \lambda_{2N}(t) \\ \vdots & \ddots & \vdots \\ \lambda_{N1}(t) & \cdots & \lambda_{NN}(t) \end{bmatrix}.$$

The individual Hamiltonian of agent i is thus defined as:

$$\mathcal{H}_i(\mathrm{x}, \boldsymbol{\lambda}_i, \mathrm{u}) = E_i(x_i) + \frac{d_i}{2}u_i^2 + \boldsymbol{\lambda}_i^\top \left(\mathrm{f(x)} + S\mathrm{x} - G(\mathrm{x})\,\mathrm{u}\right), \tag{8}$$

where $\boldsymbol{\lambda}_i^\top$ is the i-th row of Λ.

Throughout this work, we adopt the *current-value* formulation of the Hamiltonian and the adjoint variables[1] and, for notational simplicity, we continue to refer to the Hamiltonian and adjoint variables without explicitly labeling them as "current-value."

We now apply Pontryagin's Maximum Principle to each agent's optimization problem, treating the strategies of the other players as fixed. This yields the following coupled system

[1] The choice of the current-value formulation means that the exponential discount factor $e^{-\rho t}$ appearing in the cost functional is factored out of the Hamiltonian, and the discount rate ρ enters explicitly into the adjoint equations. This approach leads to a more compact expression of the optimality system.

of state, adjoint, and optimality equations, characterizing the open-loop Nash equilibrium. The full derivation of the system is provided in Appendix A.

Proposition 4 *(Characterization of open-loop Nash equilibrium) Let* $\mathrm{u}^* = (u_1^*, \ldots, u_N^*) \in \mathcal{U}^N$ *be an open-loop Nash equilibrium for the non-cooperative game (6), and let* $\mathrm{x}^*(t)$ *be the corresponding state trajectory. Then, there exists an absolutely continuous matrix of adjoint variables* $\Lambda(t) = (\lambda_{ij}(t)) \in \mathbb{R}^{N\times N}$*, such that the following system holds almost everywhere in* $[0, T]$*:*

$$
\begin{aligned}
&\dot{x}_i^*(t) = f_i(x_i^*(t)) + \sum_{j=1}^{N} \sigma_{ij}(x_j^*(t) - x_i^*(t)) - g_i(x_i^*(t))\, u_i^*(t), \quad x_i^*(0) = x_i^0,\\
&\dot{\lambda}_{ij}(t) = \rho\, \lambda_{ij}(t) - \delta_{ij} E_i'(x_i^*(t)) - \lambda_{ij}(t)\, f_j'(x_j^*(t)) + \delta_{ij} \lambda_{ij}(t)\, u_i^*(t)\, g_i'(x_i^*(t))\\
&\qquad\qquad + \sum_{k=1}^{N} \sigma_{jk}(\lambda_{ij}(t) - \lambda_{ik}(t)),\\
&\lambda_{ij}(T) = \delta_{ij} \phi_i'(x_i^*(T))\\
&u_i^*(t) = \max\left\{0, \frac{1}{d_i} \lambda_{ii}(t)\, g_i(x_i^*(t))\right\},
\end{aligned}
$$

for all $i, j = 1, \ldots, N$, where δ_{ij} denotes the Kronecker delta, which is equal to 1 when $i = j$, and 0 otherwise.

3.2 Feedback Nash equibrium

In the feedback formulation, each agent selects a control strategy of the form $u_i(t) = \varphi_i(t, \mathrm{x}(t))$, where $\varphi_i : [0, T] \times \mathbb{R}^N \to \mathbb{R}_+$ is a feedback map, depending not only on time but also on the current state of the system. We provide a classical characterization of the feedback Nash equilibrium in terms of the *current-value functions* $V_i(t, x)$, which represent the minimal discounted cost that agent i can achieve starting from state x at time t, under all admissible feedback strategies. They are defined as:

$$
V_i(t, x) := \inf_{u_i \in \mathcal{U}} \left\{ e^{-\rho T} \phi_i(x_i(T)) + \int_t^T e^{-\rho s} \left[E_i(x_i(s)) + \frac{d_i}{2} \left(u_i(t)\right)^2 \right] ds \right\}. \tag{9}
$$

Proposition 5 *(Hamilton–Jacobi–Bellman equation for feedback Nash equilibrium) Let* $V_i(t, x)$ *be the current-value function associated with agent i, as defined above, are differentiable in both variables. Then, the functions* $V_i(t, x)$ *satisfies the Hamilton–Jacobi–Bellman (HJB) equation:*

$$
\partial_t V_i(t, \mathrm{x}) - \rho\, V_i(t, \mathrm{x}) + \min_{u_i \in \mathcal{U}} \mathcal{H}_i(\mathrm{x}, \nabla_{\mathrm{x}} V_i(t, x), \mathrm{u}) = 0, \tag{10}
$$

with terminal condition:

$$
V_i(T, \mathrm{x}) = \phi_i(x_i(T)).
$$

Moreover, the optimal feedback control for agent i is obtained by minimizing the current-value Hamiltonian with respect to the control variable. It is given by:

$$\varphi_i^*(t,\mathrm{x}) = \arg\min_{u_i \in \mathcal{U}} \mathcal{H}_i\left(\mathrm{x}, \nabla_{\mathrm{x}} V_i(t,x), \mathrm{u}\right), \tag{11}$$

where the current-value Hamiltonian $\mathcal{H}_i$ is defined in Eq. 8).

Remark 1 Under regularity assumptions, and considering the structure of the Hamiltonian in Eq. 8), the minimization condition (11) yields the following explicit expression for the optimal feedback control:

$$\varphi_i^*(t,\mathrm{x}) = \max\left\{0, \frac{g_i(x_i)}{d_i}\frac{\partial V_i}{\partial x_i}(t,\mathrm{x})\right\}.$$

This expression characterizes the optimal control in feedback form as a function of the marginal value of the state and the local effectiveness of control.
While the feedback formulation offers a conceptually powerful framework, its practical implementation is often hindered by significant computational challenges. In particular, solving the coupled system of Hamilton–Jacobi–Bellman equations involves a system of nonlinear partial differential equations with interdependent value functions. Among classical numerical schemes, *semi-Lagrangian methods* have proven particularly effective for time-dependent HJB equations, thanks to their numerical stability and flexibility in handling general dynamics and control constraints; see, for instance, Falcone (2006).

In the present work, our main goal is to analyze how agents behave over a spatially structured network under different strategic scenarios (competition, cooperation, coalitions). To this end, we focus on the open-loop formulation of the game, where decisions are made at the initial time and optimal control trajectories are computed accordingly. This choice is justified by the fact that, under perfect foresight and in the absence of exogenous shocks or unexpected perturbations, the optimal open-loop strategy coincides with the feedback policy evaluated along the optimal state trajectory. Consequently, we neglect the role of state-contingent adaptation and assume that agents commit to their strategies at time zero. Extensions to genuinely adaptive feedback settings–possibly incorporating uncertainty, dynamic coalitions, or reaction to external disturbances–are left for future research.

4 Strategic interaction among agents

We now further extend the analysis to settings in which groups of agents may coordinate their actions by forming coalitions. This intermediate framework allows us to explore strategic scenarios that lie between full competition and full cooperation.

4.1 Multi-coalition game

We assume that the set of agents $\mathcal{N} = \{1, \ldots, N\}$ is partitioned into $s \geq 1$ disjoint coalitions $\mathcal{C}_1, \ldots, \mathcal{C}_s \subseteq \mathcal{N}$, such that $\bigcup_{k=1}^{s} \mathcal{C}_k = \mathcal{N}$ and $\mathcal{C}_k \cap \mathcal{C}_\ell = \emptyset$ for all $k \neq \ell$. Each coalition $\mathcal{C}_k$ includes $N_k \geq 1$ agents, and the total number of agents satisfies $\sum_{k=1}^{s} N_k = N$.

Each coalition $\mathcal{C}_k$ acts as a strategic decision-maker, jointly minimizing a collective cost functional that aggregates the individual objectives of its members:

$$J_{\mathcal{C}_k}(\mathrm{u}) = \sum_{i \in \mathcal{C}_k} J_i(\mathrm{u}), \tag{12}$$

where J_i are defined in (5), and $\mathrm{u} = (u_1, \ldots, u_N) \in \mathcal{U}^N$ is the full control vector.

A control profile u^* is a *multi-coalitional Nash equilibrium* if, for each coalition $\mathcal{C}_k$, the subvector $\mathrm{u}^*_{\mathcal{C}_k} = \{u_i^*\}_{i \in \mathcal{C}_k}$ solves:

$$\min_{\mathrm{u}_{\mathcal{C}_k} \in \mathcal{U}^{N_k}} J_{\mathcal{C}_k}(\mathrm{u}_{\mathcal{C}_k}, \mathrm{u}^*_{-\mathcal{C}_k}),$$

subject to the system dynamics (4). Here, $\mathrm{u}^*_{-\mathcal{C}_k} = (\mathrm{u}^*_{\mathcal{C}_1}, \ldots, \mathrm{u}^*_{\mathcal{C}_{k-1}}, \mathrm{u}^*_{\mathcal{C}_{k+1}}, \ldots, \mathrm{u}^*_{\mathcal{C}_s})$ denotes the collection of control strategies adopted by all coalitions other than $\mathcal{C}_k$.

For each coalition $\mathcal{C}_k$, we define the *coalitional Hamiltonian* as:

$$\mathcal{H}_{\mathcal{C}_k}(\mathrm{x}, \boldsymbol{\lambda}_{\mathcal{C}_k}, \mathrm{u}_{\mathcal{C}_k}) = \sum_{i \in \mathcal{C}_k} \left[E_i(x_i) + \frac{d_i}{2} u_i^2 \right] + \boldsymbol{\lambda}_{\mathcal{C}_k}^\top \left(\mathrm{f}(\mathrm{x}) + S\mathrm{x} - G(\mathrm{x})\, \mathrm{u} \right),$$

where $\boldsymbol{\lambda}_{\mathcal{C}_k}(t) \in \mathbb{R}^N$ is the adjoint vector associated with coalition $\mathcal{C}_k$, representing the sensitivity of its total cost with respect to the state vector $\mathrm{x}(t) \in \mathbb{R}^N$.

Proposition 6 *(Characterization of open-loop Nash equilibrium with coalitions) Let $\mathrm{u}^* = (u_1^*, \ldots, u_N^*) \in \mathcal{U}^N$ be an open-loop Nash equilibrium for the multi-coalition game, and let $\mathrm{x}^*(t)$ be the corresponding state trajectory. Then, for each coalition $\mathcal{C}_k$, there exists an absolutely continuous adjoint vector $\boldsymbol{\lambda}_{\mathcal{C}_k}(t) \in \mathbb{R}^N$ such that the following system holds almost everywhere in $[0, T]$:*

$$\begin{aligned}
&\dot{x}_i^*(t) = f_i(x_i^*(t)) + \sum_{j=1}^{N} \sigma_{ij}(x_j^*(t) - x_i^*(t)) - g_i(x_i^*(t))\, u_i^*(t), \quad x_i^*(0) = x_i^0, \quad \forall i = 1, \ldots, N, \\
&\dot{\lambda}_{\mathcal{C}_k,i}(t) = \rho\, \lambda_{\mathcal{C}_k,i}(t) - \chi_{i \in \mathcal{C}_k} \left[E_i'(x_i^*(t)) - \lambda_{\mathcal{C}_k,i}(t)\, f_i'(x_i^*(t)) + \lambda_{\mathcal{C}_k,i}(t)\, u_i^*(t)\, g_i'(x_i^*(t)) \right] \\
&\qquad\qquad + \sum_{m=1}^{N} \sigma_{im} \left(\lambda_{\mathcal{C}_k,i}(t) - \lambda_{\mathcal{C}_k,m}(t) \right), \quad \forall i = 1, \ldots, N_k, \ \forall k = 1, \ldots, s, \\
&\lambda_{\mathcal{C}_k,i}(T) = \chi_{i \in \mathcal{C}_k} \phi_i'(x_i^*(T)), \quad \forall i = 1, \ldots, N_k, \ \forall k = 1, \ldots, s, \\
&u_i^*(t) = \max \left\{ 0, \ \sum_{k=1}^{s} \chi_{i \in \mathcal{C}_k} \frac{1}{d_i} \lambda_{\mathcal{C}_k,i}(t)\, g_i(x_i^*(t)) \right\}, \quad \forall i = 1, \ldots, N.
\end{aligned} \tag{13}$$

Here, $\lambda_{\mathcal{C}_k,i}(t)$ denotes the i-th component of the adjoint vector $\boldsymbol{\lambda}_{\mathcal{C}_k}(t)$, associated with coalition $\mathcal{C}_k$, and $\chi_{i \in \mathcal{C}_k}$ is the indicator function, which is equal to 1 if agent j belongs to the coalition $\mathcal{C}_k$, and 0 otherwise.

The proof is omitted to avoid repetition, as it follows the same structure as in the non-cooperative case. The multi-coalition framework generalizes both fully competitive and fully cooperative settings, as it includes the following cases:

- When $s = N$, each agent forms a singleton coalition: this recovers the purely non-cooperative game.
- When $s = 1$, all agents form a single coalition: this corresponds to the socially optimal (centralized) solution.
- Intermediate values of s allow for modeling *partial cooperation* among agents.

4.2 Full cooperation

The case of full cooperation corresponds to the situation where all agents belong to a single coalition, that is, $s = 1$ and $\mathcal{C}_1 = \mathcal{N}$. In this case, the game reduces to a centralized optimal control problem, where a single planner aims to minimize the total cost over the entire system:

$$\min_{\mathrm{u}\in\mathcal{U}^N} \sum_{i=1}^{N} J_i(\mathrm{u}),$$

subject to the system dynamics (4).

The corresponding optimality system is obtained by setting $\mathcal{C}_1 = \mathcal{N}$ in Proposition 6, and consists of a state-adjoint-control triple $(\mathrm{x}^*, \boldsymbol{\lambda}, \mathrm{u}^*)$ satisfying:

$$\dot{x}_i^*(t) = f_i(x_i^*(t)) + \sum_{j=1}^{N} \sigma_{ij}(x_j^*(t) - x_i^*(t)) - g_i(x_i^*(t))\, u_i^*(t), \quad x_i^*(0) = x_i^0,$$

$$\dot{\lambda}_i(t) = \rho\, \lambda_i(t) - E_i'(x_i^*(t)) + \lambda_i(t)\, [f_i'(x_i^*(t)) - u_i^*(t) g_i'(x_i^*(t))] + \sum_{j=1}^{N} \sigma_{ij}(\lambda_i(t) - \lambda_j(t)),$$

$$\lambda_i(T) = \phi_i'(x_i^*(T)),$$

$$u_i^*(t) = \max\left\{0,\ \frac{1}{d_i}\lambda_i(t)\, g_i(x_i^*(t))\right\}, \quad \forall i = 1, \ldots, N.$$

5 Cooperative cost allocation

In cooperative control scenarios involving multiple stakeholders–such as regional authorities, landowners, or environmental agencies–coordinated strategies typically lead to greater efficiency. However, this raises a fundamental question: how should the total cost of cooperation be fairly allocated among participants?

When agents differ in ecological vulnerability, control capacity, and spatial influence, cost-sharing becomes both technically and politically challenging. While cooperation often reduces total system-wide costs, it may not benefit every agent individually. Some may

face higher costs than under non-cooperative strategies, which can discourage participation unless costs are redistributed fairly. A meaningful allocation should reflect each agent's ecological exposure, strategic role in the spatial network, and contribution to the collective outcome. It must also account for indirect benefits, such as the lowered risk of reinfestation resulting from the efforts of others, and the difficulty of assigning value to passive protection.

We consider the problem of allocating costs within cooperative settings that may involve full or partial coalitions. In each case, once a coalition or coalition structure adopts a cooperative control strategy, the goal is to determine how to share the resulting cost in a fair and incentive-compatible way. We present two approaches grounded in cooperative game theory, both applied *a posteriori* to a known cooperative outcome. The first is the *Nash bargaining solution*, which distributes the cooperative gains relative to non-cooperative baselines. The second is the *Myerson value*, a generalization of the Shapley value that accounts for externalities across coalitions and allocates costs based on marginal contributions in a spatially structured system.

5.1 Surplus sharing with bargaining power: the Nash bargaining solution

The Nash bargaining solution provides a method for allocating the total cooperative cost by using each agent's disagreement point, corresponding to the cost that an agent would incur in the absence of cooperation, i.e., if the agent were to act independently within a non-cooperative environment.

Let J_i^{NC} denote the cost incurred by agent $i = 1, \ldots, N$ in the non-cooperative setting, and let J^{C} be the total cost achieved under full cooperation, that is, when all agents coordinate to minimize the sum of individual costs. We assume that cooperation is beneficial for the group as a whole, meaning that $J^{\mathrm{C}} < \sum_{i=1}^{N} J_i^{\mathrm{NC}}$. This condition ensures a positive cooperative surplus, which can then be redistributed among the agents. We define the cooperative surplus as

$$\Delta := \sum_{i=1}^{N} J_i^{\mathrm{NC}} - J^{\mathrm{C}} > 0, \tag{14}$$

which represents the total gain from cooperation.

To account for differences in bargaining power or perceived contribution, we assign to each agent i a weight $\alpha_i > 0$, with $\sum_{i=1}^{N} \alpha_i = 1$. The Nash bargaining solution is then obtained by maximizing a weighted product of individual gains, where each gain is defined as the difference between the agent's non-cooperative cost and their assigned cooperative cost. The resulting optimization problem is:

$$\max_{0 \le c_i < J_i^{\mathrm{NC}}} \prod_{i=1}^{N} \left(J_i^{\mathrm{NC}} - c_i \right)^{\alpha_i}, \quad \text{subject to} \quad \sum_{i=1}^{N} c_i = J^{\mathrm{C}}. \tag{15}$$

The upper bound $c_i < J_i^{\mathrm{NC}}$ ensures that each agent achieves a strictly lower cost compared to the non-cooperative scenario, thereby preserving *individual rationality*. The lower bound $c_i \geq 0$ ensures that each agent contributes positively to the collective effort and avoids being subsidized. Together, these constraints define a feasible and equitable redistribution of the cooperative cost. This solution is Pareto efficient within the coalition, meaning that no alternative allocation can improve one agent's outcome without worsening another's. Moreover, the assigned cost shares reflect the relative benefits each agent gains from cooperating, with those who save more contributing proportionally more to the total cost.

We denote by c_i^{NB} the cost allocated to agent i as a result of the bargaining process. The following proposition, whose proof is provided in Appendix A, characterizes the unique solution to the Nash bargaining problem, showing that each agent pays its non-cooperative cost minus a share of the collective surplus, proportionally to their bargaining weight α_i.

Proposition 7 *Problem (15) admits a unique optimal solution. The optimal cost allocation is given in closed form by:*

$$c_i^{\mathrm{NB}} = J_i^{\mathrm{NC}} - \alpha_i \Delta, \quad foralli = 1, \ldots, N, \tag{16}$$

where Δ is the cooperative surplus defined in (14).

The final allocation formula in (16) represents the division of the cooperative surplus among the agents, where each agent's share depends on their bargaining weight α_i. When the bargaining weights are equal, i.e., $\alpha_i = 1/N$, the surplus is distributed equally among the agents. However, when the bargaining weights differ, the allocation reflects the relative bargaining power of each agent, with those having higher bargaining power (larger α_i) receiving a larger share of the total surplus.

5.2 Coalition-aware cost allocation: the Myerson value

The Nash bargaining solution offers a fair and tractable rule for allocating costs within any cooperating group, whether it includes all agents or only a subset forming a coalition. It compares the cooperative outcome to a fixed non-cooperative baseline and distributes the surplus based on individual improvements. However, this approach treats each coalition in isolation, without accounting for the influence of agents outside the group. In networked ecological systems, this limitation is significant: the outcome for a coalition often depends on the strategies adopted by others. For example, control efforts by neighboring regions may reduce reinfestation risk, while inaction elsewhere may undermine local interventions. These *externalities* are not captured by coalition-by-coalition bargaining.

To address this limitation, we adopt the more general framework of *games in partition function form*, introduced by Thrall and Lucas (1963), where the value of a coalition depends not only on its members but also on how the rest of the agents are organized.

Within this setting, the *Myerson value* (Myerson, 1977) provides a principled allocation rule that extends the classical *Shapley value* (Shapley, 1953), which assumes that coalitions operate independently. The Myerson value assigns to each agent a share of the total cost based on their average marginal contribution across all coalitions and partitions of the system, thus incorporating the strategic interdependence among groups.

Let $\mathcal{N} = \{1, 2, \ldots, N\}$ be the set of players, and let Π denote the set of all partitions of $\mathcal{N}$. An *embedded coalition* is a pair $(\mathcal{C}, \mathcal{P})$, where $\mathcal{P} \in \Pi$ is a partition of the player set $\mathcal{N}$, and $\mathcal{C} \in \mathcal{P}$ is a coalition belonging to that partition. The set of all embedded coalitions is denoted by

$$\mathcal{E} = \{(\mathcal{C}, \mathcal{P}) \mid \mathcal{P} \in \Pi,\ \mathcal{C} \in \mathcal{P}\}.$$

A *partition function* $\mathcal{V}$ is a map $\mathcal{V} : \mathcal{E} \to \mathbb{R}$, which assigns a real value $\mathcal{V}(\mathcal{C}, \mathcal{P})$ to each embedded coalition $(\mathcal{C}, \mathcal{P}) \in \mathcal{E}$. The quantity $\mathcal{V}(\mathcal{C}, \mathcal{P})$ represents the value generated by the coalition $\mathcal{C}$ when the entire set of players $\mathcal{N}$ is organized according to the partition $\mathcal{P}$.

The Myerson value (Myerson, 1977) for player i is defined as

$$\psi_i(\mathcal{V}) = \sum_{(\mathcal{C},\mathcal{P})\in\mathcal{E}} (-1)^{|\mathcal{P}|-1}\,(|\mathcal{P}|-1)!\left(\frac{1}{N} - \omega_i(\mathcal{C},\mathcal{P})\right)\mathcal{V}(\mathcal{C},\mathcal{P}), \tag{17}$$

where the correction terms $\omega_i(\mathcal{C}, \mathcal{P})$ are given by

$$\omega_i(\mathcal{C},\mathcal{P}) = \sum_{\substack{\mathcal{D}\in\mathcal{P}\\ \mathcal{D}\neq\mathcal{C}\, i\notin\mathcal{D}}} \frac{1}{(|\mathcal{P}|-1)(N-|\mathcal{D}|)}.$$

These terms adjust the baseline share $1/N$ by accounting for the influence of external coalitions that do not include player i. Specifically, they aggregate the impact of such external groups, assigning to each a weight inversely proportional to its size to reflect the greater potential influence of smaller coalitions.

The Myerson value satisfies the axioms of Anonymity, Carrier, and Additivity,[2] and is uniquely characterized by these properties, providing a consistent and equitable rule for allocating costs while accounting for the structure of externalities among players (Kóczy, 2018).

Remark 2 In the case of full cooperation $(\mathcal{N}, \{\mathcal{N}\})$, the correction terms vanish, that is,

$$\omega_i(\mathcal{N}, \{\mathcal{N}\}) = 0 \quad \text{for all} \quad i \in \mathcal{N},$$

since there are no external coalitions in the partition. As a consequence, the Myerson values can be rewritten as

$$\psi_i(\mathcal{V}) = \frac{1}{N}\mathcal{V}(\mathcal{N}, \{\mathcal{N}\}) + \sum_{\substack{(\mathcal{C},\mathcal{P})\in\mathcal{E}\\ (\mathcal{C},\mathcal{P})\neq(\mathcal{N},\{\mathcal{N}\})}} (-1)^{|\mathcal{P}|-1}\left(\frac{1}{N} - \omega_i(\mathcal{C},\mathcal{P})\right)\mathcal{V}(\mathcal{C},\mathcal{P}). \tag{18}$$

[2] Anonymity requires that players who contribute identically to all coalitions are treated equally. Carrier states that players who do not affect the value of any coalition must receive a zero payoff. Additivity ensures that if two partition function games are combined, the allocation in the combined game equals the sum of the allocations in each individual game.

This decomposition explicitly separates the contribution from full cooperation from the correction terms induced by externalities across coalitions.

The following proposition states that the sum of the individual Myerson values exactly recovers the value of the grand coalition. The proof is provided in Appendix A.

Proposition 8 *The sum of the individual Myerson values is:*

$$\sum_{i=1}^{N} \psi_i(\mathcal{V}) = \mathcal{V}(\mathcal{N}, \{\mathcal{N}\}).$$

Based on this property, we can define a consistent allocation rule among players. Each value $\psi_i(\mathcal{V})$ represents the share of the total cost allocated to player i. Thus, the vector

$$(\psi_1(\mathcal{V}), \psi_2(\mathcal{V}), \ldots, \psi_N(\mathcal{V}))$$

provides a complete allocation of the system's total cost among the agents, reflecting the cooperative structure of the model and consistently accounting for externalities. This allocation refers to the fully cooperative scenario where all players act together to minimize the total cost, while the externalities arising from the organization of the system into different coalitions are properly considered.

Remark 3 The Myerson allocation $\psi_i(\mathcal{V})$ and the Nash bargaining solution c_i^{NB} in (16) are connected through bargaining weights α_i^M, defined as

$$\alpha_i^M = \frac{1}{\Delta}\left(J_i^{\mathrm{NC}} - \psi_i(\mathcal{V})\right), \tag{19}$$

where Δ is the cooperative surplus defined in (14). These weights reflect each agent's contribution to the cooperative surplus, with higher bargaining power assigned to agents whose cooperation leads to greater cost reductions. While the Nash bargaining solution assigns bargaining powers exogenously, the Myerson value incorporates them endogenously, based on marginal contributions. In contrast, the Nash solution uses fixed bargaining powers, resulting in a simpler but less flexible allocation.

In our framework, the value $\mathcal{V}(\mathcal{C}, \mathcal{P})$ of an embedded coalition $(\mathcal{C}, \mathcal{P})$ is computed based on the multi-coalition dynamic game described in Sect. 4.1, where each coalition acts as a strategic decision-maker minimizing its aggregated cost functional.

Given a partition $\mathcal{P} = \{\mathcal{C}_1, \ldots, \mathcal{C}_s\} \in \Pi$, we solve for the open-loop Nash equilibrium $\mathrm{u}^*_{\mathcal{P}}$ associated with $\mathcal{P}$, leading to the equilibrium state trajectory $\mathrm{x}^*_{\mathcal{P}}(t)$. The equilibrium pair $(\mathrm{x}^*_{\mathcal{P}}, \mathrm{u}^*_{\mathcal{P}})$ is characterized by the system of state dynamics, adjoint equations, and optimality conditions described in Proposition 6. Then, we define $\mathcal{V}(\mathcal{C}_k, \mathcal{P})$ as the aggregate cost of the coalition $\mathcal{C}_k$ evaluated along the equilibrium trajectory associated with the partition $\mathcal{P}$, that is,

$$\mathcal{V}(\mathcal{C}_k, \mathcal{P}) = J_{\mathcal{C}_k}(\mathrm{u}^*_{\mathcal{P}}), \tag{20}$$

where $J_{\mathcal{C}_k}(\mathrm{u})$ is defined in (12).

Two-player game

For $N = 2$, denoting by J_1^{NC} and J_2^{NC} the non-cooperative costs of players 1 and 2, respectively, and by J^{C} the cooperative cost of the grand coalition, we have

$$J_1^{\mathrm{NC}} = \mathcal{V}(\{1\},\{\{1\},\{2\}\}), \quad J_2^{\mathrm{NC}} = \mathcal{V}(\{2\},\{\{1\},\{2\}\}), \quad J^{\mathrm{C}} = \mathcal{V}(\{1,2\},\{\{1,2\}\}).$$

The Myerson values are then explicitly given by

$$\psi_1(\mathcal{V}) = \frac{1}{2}\left(J^{\mathrm{C}} + J_1^{\mathrm{NC}} - J_2^{\mathrm{NC}}\right), \quad \psi_2(\mathcal{V}) = \frac{1}{2}\left(J^{\mathrm{C}} + J_2^{\mathrm{NC}} - J_1^{\mathrm{NC}}\right),$$

and they coincide with the Nash bargaining cost allocation c_i^{NB} in (16) when the bargaining weights are equal, i.e., $\alpha_1^M = \alpha_2^M = 1/2$. This was expected, as there are no marginal coalitions to consider, and the surplus is thus equally distributed between the two players.

Three-player game

For a three-player game $\mathcal{N} = \{1,2,3\}$, the Myerson values can be explicitly computed as:

$$\begin{aligned}
\psi_1(\mathcal{V}) = {} & \frac{1}{3}\mathcal{V}(\{1,2,3\},\{\{1,2,3\}\}) - \frac{1}{3}\mathcal{V}(\{1\},\{\{1\},\{2\},\{3\}\}) \\
& + \frac{1}{6}\mathcal{V}(\{1,2\},\{\{1,2\},\{3\}\}) - \frac{1}{3}\mathcal{V}(\{3\},\{\{1,2\},\{3\}\}) \\
& + \frac{1}{6}\mathcal{V}(\{1,3\},\{\{1,3\},\{2\}\}) - \frac{1}{3}\mathcal{V}(\{2\},\{\{1,3\},\{2\}\}) \\
& + \frac{2}{3}\mathcal{V}(\{1\},\{\{1\},\{2,3\}\}) - \frac{1}{3}\mathcal{V}(\{2,3\},\{\{1\},\{2,3\}\}) \\
& + \frac{1}{6}\mathcal{V}(\{2\},\{\{1\},\{2\},\{3\}\}) + \frac{1}{6}\mathcal{V}(\{3\},\{\{1\},\{2\},\{3\}\}),
\end{aligned} \tag{21}$$

$$\begin{aligned}
\psi_2(\mathcal{V}) = {} & \frac{1}{3}\mathcal{V}(\{1,2,3\},\{\{1,2,3\}\}) - \frac{1}{3}\mathcal{V}(\{2\},\{\{1\},\{2\},\{3\}\}) \\
& + \frac{1}{6}\mathcal{V}(\{1,2\},\{\{1,2\},\{3\}\}) - \frac{1}{3}\mathcal{V}(\{3\},\{\{1,2\},\{3\}\}) \\
& + \frac{1}{6}\mathcal{V}(\{2,3\},\{\{2,3\},\{1\}\}) - \frac{1}{3}\mathcal{V}(\{1\},\{\{2,3\},\{1\}\}) \\
& + \frac{2}{3}\mathcal{V}(\{2\},\{\{2\},\{1,3\}\}) - \frac{1}{3}\mathcal{V}(\{1,3\},\{\{2\},\{1,3\}\}) \\
& + \frac{1}{6}\mathcal{V}(\{1\},\{\{1\},\{2\},\{3\}\}) + \frac{1}{6}\mathcal{V}(\{3\},\{\{1\},\{2\},\{3\}\}),
\end{aligned} \tag{22}$$

$$\begin{aligned}\psi_3(\mathcal{V}) = &\frac{1}{3}\mathcal{V}(\{1,2,3\},\{\{1,2,3\}\}) - \frac{1}{3}\mathcal{V}(\{3\},\{\{1\},\{2\},\{3\}\})\\ &+ \frac{1}{6}\mathcal{V}(\{1,3\},\{\{1,3\},\{2\}\}) - \frac{1}{3}\mathcal{V}(\{2\},\{\{1,3\},\{2\}\})\\ &+ \frac{1}{6}\mathcal{V}(\{2,3\},\{\{2,3\},\{1\}\}) - \frac{1}{3}\mathcal{V}(\{1\},\{\{2,3\},\{1\}\})\\ &+ \frac{2}{3}\mathcal{V}(\{3\},\{\{3\},\{1,2\}\}) - \frac{1}{3}\mathcal{V}(\{1,2\},\{\{3\},\{1,2\}\})\\ &+ \frac{1}{6}\mathcal{V}(\{1\},\{\{1\},\{2\},\{3\}\}) + \frac{1}{6}\mathcal{V}(\{2\},\{\{1\},\{2\},\{3\}\}).\end{aligned} \tag{23}$$

For a three-player system, the computation of the Myerson values requires solving 5 dynamic problems of the form (13), each corresponding to one of the possible partitions of the set $\{1,2,3\}$. For each partition $\mathcal{P}$, the associated open-loop Nash equilibrium yields the state–control trajectory $(\mathrm{x}^*_{\mathcal{P}}, \mathrm{u}^*_{\mathcal{P}})$, from which we compute the values $\mathcal{V}(\mathcal{C},\mathcal{P})$ for every coalition $\mathcal{C} \in \mathcal{P}$, as in (20).

The full computational procedure for a three-player game is detailed in the Supplementary Information file, where we report the algorithm used to compute the Myerson values. For solving the forward–backward optimality system associated with each coalition structure, classical numerical solvers such as bvp4c in MATLAB can be employed. However, due to the Hamiltonian structure of the problem and the presence of both initial and terminal conditions, *ad hoc* numerical schemes, such as symplectic integrators, are often required to effectively handle the coupling and ensure long-term numerical stability (Martiradonna et al., 2020).

For larger systems, the computational burden of computing the Myerson values increases rapidly. The number of partitions of the agent set $\mathcal{N}$, given by the Bell number B_N, grows more than exponentially with N, and each partition requires solving a separate forward–backward optimality system. As a result, the total number of dynamic problems increases sharply with the number of agents, leading to a steep rise in overall computational cost, both in terms of memory usage and runtime. To address this issue, we plan to employ model order reduction techniques (Schilders et al., 2008) to efficiently approximate both forward–backward optimality systems and feedback equilibria, preserving the key system dynamics at a significantly lower computational cost. In parallel, data-driven surrogate models, including Physics-Informed Neural Networks (PINNs) (Cuomo et al., 2022), offer a promising direction.

6 Numerical simulations

In this section, we present a numerical study to explore the main features of the model and the resulting dynamic behaviors within a three-node network. To this end, we introduce explicit functional forms for the biological processes and cost structures, and set up a symmetric baseline configuration from which sensitivity analyses will be developed.

6.1 Model specifications

Recalling that the local population dynamics in each area follow the general form (3), we adopt the following specific assumptions inspired by Baker et al. (2023), where the spread of *Ailanthus altissima* was modeled under the control of a single central authority.

In this context, we consider a more general setting involving a hypothetical invasive species spreading over a heterogeneous landscape partitioned into multiple management areas, each controlled by a distinct local decision maker. Each agent independently implements its own control strategy, with the possibility to strategically interact within a non-cooperative dynamic game framework. This approach enables us to investigate how spatial structure, ecological heterogeneity, and decentralized decision-making influence invasion dynamics and the potential advantages of cooperation.

As in Baker et al. (2023), ecological heterogeneity is captured through area-specific habitat suitability indices $h_i \in [0, 1]$, which modulate the intrinsic growth rate of the invasive species in each management area. Those ones with higher habitat suitability offer more favorable conditions for species diffusion, leading to faster local growth, while less suitable areas impose natural limitations on expansion. These differences introduce asymmetries in the local invasion pressure faced by agents, and consequently affect both their control efforts and their strategic interactions within the network.

Building on these observations, we specify the following functional forms for the biological processes and cost components:

- The intrinsic growth of the invasive species is described by a logistic-like function modulated by a habitat suitability index $h_i \in [0, 1]$:

$$f_i(x_i) = r\, x_i \left(h_i - \frac{x_i}{K} \right),$$

where $r > 0$ is the intrinsic growth rate and $K > 0$ the carrying capacity.

- The effectiveness of the control action is modeled through a type-II functional response:

$$g_i(x_i) = \frac{\mu\, x_i}{1 + \tau\, \mu\, x_i},$$

where $\mu > 0$ denotes the maximum removal area per individual per year, and $\tau > 0$ represents the average time scale for the onset of saturation effects.

- The indirect damage cost incurred by each agent due to the presence of the invasive species is quadratic in the local population size:

$$E_i(x_i) = \gamma_i^{(1)} x_i + \gamma_i^{(2)} x_i^2,$$

with coefficients $\gamma_i^{(1)}, \gamma_i^{(2)} \geq 0$ representing linear and nonlinear components of ecological and economic damages.

- The terminal environmental damage cost is proportional to the remaining population at the final time:

$$\phi_i(x_i) = \beta_i x_i,$$

where $\beta_i \geq 0$ weights the final residual infestation.

6.2 Baseline parameterization

We first consider a fully symmetric configuration across the three areas, in order to isolate and understand the impact of specific parameters when later introducing asymmetries. The parameter values used in the baseline scenario are summarized in Table 1. They represent a hypothetical invasive species with traits broadly characteristic of fast-spreading plant or animal invaders commonly found in fragmented landscapes.

Starting from this baseline setting, we perform a sensitivity analysis by introducing asymmetries in habitat suitability, control costs, and diffusion rates to assess their impact on strategic interactions and the value of cooperation.

6.3 Sensitivity analysis

To systematically investigate how economic heterogeneity and spatial externalities affect optimal management strategies and the value of cooperation, we conduct a sensitivity analysis on crucial parameters of the model. Starting from the fully symmetric baseline configuration described earlier, we introduce controlled perturbations to specific parameters governing diffusion, control costs, and habitat suitability. For each perturbed scenario, we

Table 1 Baseline parameter values for the symmetric three-node model

Parameter	Value	Unit	Description
r	0.15	year^{-1}	Intrinsic growth rate
K	1000	individuals/km^2	Carrying capacity
h_i	1.0	dimensionless	Habitat suitability index
μ	0.3	year^{-1}	Maximum per capita removal rate
τ	0.01	km$^2\times$ year / individual	Control saturation parameter
$\gamma_1^{(i)}$	7	€/(individual $\times$ year)	Linear damage cost coefficient
$\gamma_2^{(i)}$	0.015	€/(individual$^2\times$ year)	Quadratic damage cost coefficient
β_i	7	€/individual	Terminal damage cost coefficient
d_i	11000	€ $\times$ year	Control effort cost coefficient
ρ	0.05	year^{-1}	Discount rate
σ_{ij}	0.5	year^{-1}	Diffusion rate between areas
$x_i(0)$	300	individuals/km^2	Initial population density
T	10	years	Time horizon

compare the outcomes under two strategic settings: decentralized management (non-cooperative game) and full cooperation among agents.

Our analysis focuses on two main performance indicators: the *cooperation gain* (%), defined as the relative reduction in total discounted costs achieved under full cooperation compared to the non-cooperative setting,

$$\text{Cooperation Gain} = \frac{\sum_{i=1}^{3} J_i^{\text{NC}} - J^{\text{C}}}{\sum_{i=1}^{3} J_i^{\text{NC}}} \times 100, \tag{24}$$

where J_i^{NC} denotes the individual cost incurred by agent i under non-cooperation, and J^{C} is the total cost under full cooperation; and the *total population reduction* (%), defined as the percentage decrease in the final aggregate population across all areas due to cooperation,

$$\text{Total Population Reduction} = \frac{\sum_{i=1}^{3} x_i^{\text{NC}}(T) - \sum_{i=1}^{3} x_i^{\text{C}}(T)}{\sum_{i=1}^{3} x_i^{\text{NC}}(T)} \times 100, \tag{25}$$

where $x_i^{\text{NC}}(T)$ and $x_i^{\text{C}}(T)$ denote the final population densities at the terminal time T under non-cooperation and cooperation, respectively.

We focus on quantifying the effects of parameter variations on cooperation gains and population outcomes because cooperation represents a key mechanism for improving the collective efficiency of control strategies in fragmented landscapes. Identifying conditions under which cooperation becomes most valuable is crucial for informing policy interventions and resource-sharing agreements among local decision makers. In particular, understanding how ecological and economic heterogeneity amplify or mitigate the benefits of cooperation provides actionable insights into when and where coordinated efforts are most needed to effectively manage biological invasions.

We first analyze the sensitivity of these indicators to variations in the diffusion rates σ_{ij}, which regulate species mobility across regions. Further, we investigate the effects of heterogeneity in the control effort costs d_i, which affect local economic incentives for population management. Finally, we explore the role of habitat suitability indices h_i, which modulate the intrinsic growth potential of the invasive population across different areas. In each case, we vary two parameters independently while keeping all others as fixed at their baseline values reported in Table 1.

Variation of diffusion rates σ_{ij}

The diffusion coefficients σ_{ij} regulate the spatial coupling between areas by modeling the motion intensity of the invasive species across the network. We now examine how the degree of spatial connectivity influences the invasion control's dynamics and the strategic benefits of cooperation.

Starting from the symmetric baseline configuration reported in Table 1, we perform a two-dimensional sensitivity analysis by varying two diffusion coefficients, σ_{12} and σ_{13}, while keeping the third connection, σ_{23}, fixed at its baseline value $\sigma_{23} = 0.5\ \text{year}^{-1}$. Specifically, σ_{12} and σ_{13} are independently varied over the interval $[0, 1]\ \text{year}^{-1}$ to explore different levels of spatial coupling between areas 1–2 and 1–3.

Figure 2 summarizes the results of this sensitivity analysis. The left panel displays the cooperation gain (%) as a function of σ_{12} and σ_{13}, while the right panel shows the corresponding total population reduction (%). The results indicate that both the cooperation gain

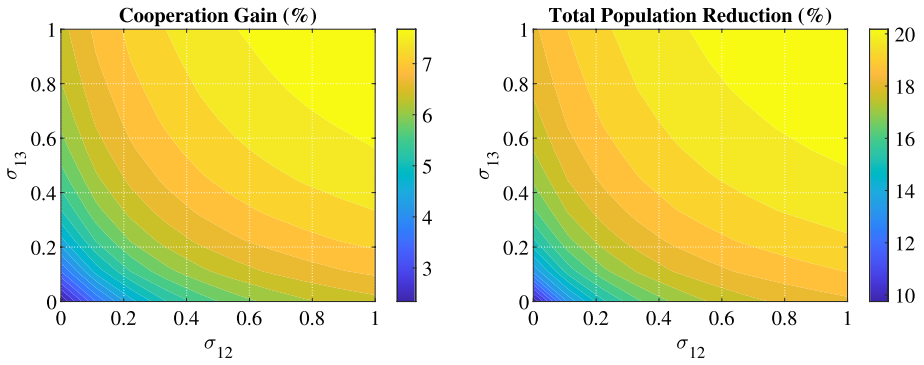

Fig. 2 Effects of varying the diffusion coefficients σ_{12} and σ_{13} on the system outcomes, with σ_{23} fixed at 0.5 year^{-1}. Left: cooperation gain (%) measured as the relative reduction in total cost achieved under full cooperation compared to the non-cooperative case. Right: total population reduction (%) at the final time $T = 10$ years, achieved through cooperation. All other parameters are set according to the baseline configuration reported in Table 1

and the total population reduction exhibit a positive relationship with the diffusion rates σ_{12} and σ_{13}. In regimes of low spatial connectivity (small values of σ_{ij}), areas behave quasi-independently, resulting in bounded strategic externalities and poor cooperation benefits: the cooperation gain remains below 5%, and the associated population reduction is negligible. As diffusion rates increase, spatial interactions become more pronounced, amplifying the mutual influence of control actions across areas.

In particular, when σ_{12} and σ_{13} approach 1, the cooperation gain exceeds 7% and the total final population reduction approaches 20%, highlighting the critical role of spatial spillovers in enhancing the value of coordinated strategies.

However, the dependence of both indicators on the diffusion parameters is nonlinear. In fact, while the cooperation gain and the population reduction increase monotonically with σ_{ij}, the marginal benefits of enhanced connectivity exhibit diminishing returns beyond intermediate diffusion levels ($\sigma_{ij} \gtrsim 0.5$). This behavior suggests the existence of a threshold effect: moderate spatial coupling substantially increases the strategic advantage of cooperation, whereas the additional gains become progressively marginal as the connectivity approaches high levels.

These findings emphasize that the design and promotion of cooperative control efforts should particularly target systems with intermediate spatial interactions, where the potential gains are both significant and sensitive to changes in connectivity.

Variation of control cost parameters d_i

We now explore how differences in local control costs affect the dynamics of invasion control and the benefits of cooperation. In line with the approach adopted for the diffusion coefficients, we perform a two-dimensional sensitivity analysis by varying the control cost parameters d_1 and d_2 independently over the interval $[5000, 20000]$ euro $\times$ year, while keeping d_3 fixed at its baseline value of 11000 euro $\times$ year.

For each combination (d_1, d_2), we solve the optimal control problems under both non-cooperative and fully cooperative strategic settings. The cooperation gain and the total population reduction are computed as defined in (24) and (25), allowing a direct comparison of the effects induced by economic versus spatial asymmetries.

The results are summarized in Fig. 3. The left panel reports the cooperation gain (%) as d_1 and d_2 vary, while the right panel shows the total population reduction (%) at the final time T. The results reveal that since d_1 and d_2 differ significantly, cooperation enables agents to reallocate efforts towards the areas where control is less costly, thereby achieving substantial savings compared to the decentralized outcome.

The total population reduction follows a complementary pattern, being larger when the costs d_1 and d_2 are both low. In such cases, control efforts are more intense overall, enabling a more effective control of the invasive species. Conversely, when both costs are high, agents tend to reduce their efforts, resulting in a smaller reduction of the total population, even under cooperation.

As observed for the diffusion coefficients, the relationship between control costs and system performance is nonlinear. Marginal increases in control costs at low baseline values produce moderate impacts, while increases beyond certain thresholds trigger sharp declines in control intensity, thereby amplifying the relative benefits of cooperation. This phenomenon then highlights the role of cost asymmetries as a critical driver of strategic complementarities among agents.

Variation of habitat suitability h_i

We next investigate how heterogeneity in local habitat quality influences system outcomes and the benefits of cooperation. Habitat suitability parameters h_i directly drive the intrinsic growth of the invasive population in each area, affecting both local dynamics and spillovers among areas.

Starting from the symmetric baseline configuration, we perform a two-dimensional sensitivity analysis by varying h_1 and h_2 independently in the interval $[0, 1]$, while keeping h_3 fixed at its baseline value $h_3 = 1.0$. This setting allows us to capture a range of ecological conditions, from poor-quality habitats (low h_i) to highly suitable environments (high h_i).

Figure 4 reports the resulting cooperation gain and total population reduction. Both indicators display a significant positive dependence on the habitat suitability indices: higher values of h_1 and h_2 lead to stronger cooperation gains and greater reductions in final population size. When h_1 and h_2 are low, the invasion dynamics are naturally weak, resulting in limited room for improvement through coordinated strategies: cooperation gains remain below 5%, and the final population reduction does not exceed 15%. Conversely, as habitat suitability increases, the invasive species proliferates more rapidly, enhancing the potential

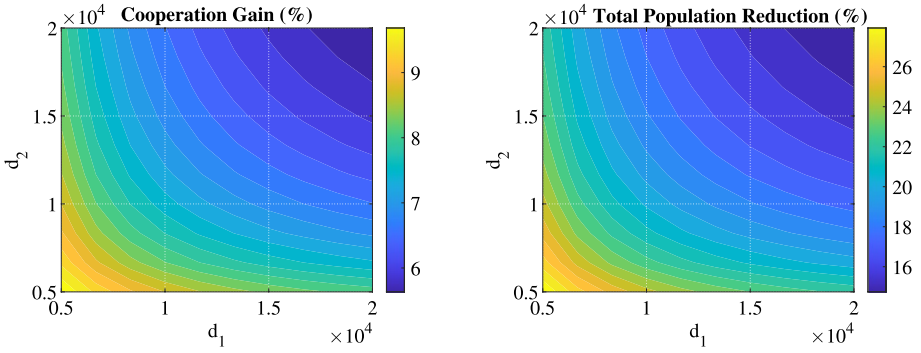

Fig. 3 Effects of varying the control costs d_1 and d_2, with d_3 fixed at 11000 euro × year. Left: cooperation gain (%) relative to the non-cooperative baseline. Right: total population reduction (%) achieved through cooperation. All other parameters are set according to the baseline configuration in Table 1

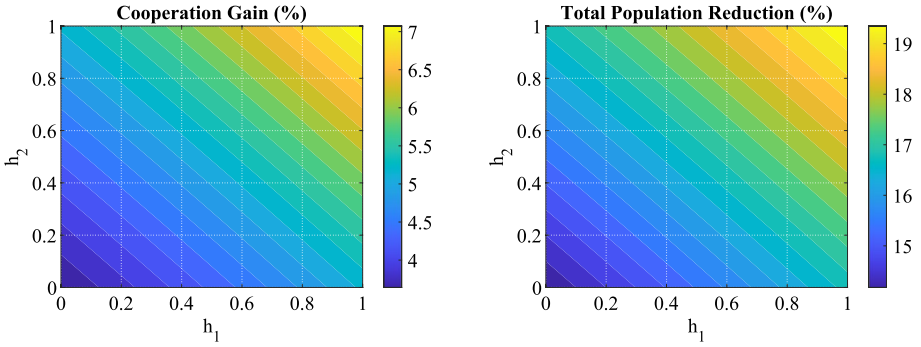

Fig. 4 Effects of varying habitat suitability parameters h_1 and h_2, with h_3 fixed at 1.0. Left: cooperation gain (%). Right: total population reduction (%) at final time $T = 10$ years. Other parameters are set according to the baseline configuration in Table 1

benefits of cooperation. When both h_1 and h_2 approach 1, the cooperation gain reaches 7% and the total population reduction exceeds 18%.

These results highlight that cooperative control becomes particularly favorable in highly suitable landscapes, where population growth is more intense and externalities between areas are amplified. The nearly symmetric and linear patterns observed suggest that improvements in either h_1 or h_2 contribute comparably to the overall outcomes, underlining the relevance of considering landscape heterogeneity when designing cooperative management policies.

6.4 Allocation of control costs in a heterogeneous landscape

We now consider a scenario featuring three heterogeneous areas, associated with distinct land-use types, over a planning horizon of $T = 10$ years. Each area differs in its ecological conditions, potential economic damages, and cost structure. More specifically, we consider the following types of area:

- *Area 1* (natural reserve) represents a highly suitable habitat for the invasive species, with moderate levels of economic damages and control costs.
- *Area 2* (agricultural zone) is characterized by lower habitat suitability but higher potential economic damages, reflecting the high value and vulnerability of agricultural activities. It also faces comparatively higher control costs.
- *Area 3* (peri-urban area) presents intermediate ecological conditions and moderate economic impacts, combining features of both natural and anthropogenic environments.

The parameters defining the ecological and economic features of each area are summarized in Table 2.

Spatial interactions between areas are modeled through the diffusion matrix

$$S = \begin{bmatrix} 0 & 0.5 & 0.3 \\ 0.5 & 0 & 0.4 \\ 0.3 & 0.4 & 0 \end{bmatrix},$$

Table 2 Ecological and economic parameters for the three heterogeneous areas

Parameter	Area 1 (Natural reserve)	Area 2 (Agricultural zone)	Area 3 (Peri-urban area)
Habitat suitability h_i	0.9	0.7	0.8
Linear damage coefficient $\gamma_1^{(i)}$	2	5	3
Quadratic damage coefficient $\gamma_2^{(i)}$	0.01	0.02	0.015
Terminal cost coefficient β_i	5	3	4
Control cost coefficient d_i	10000	12000	11000

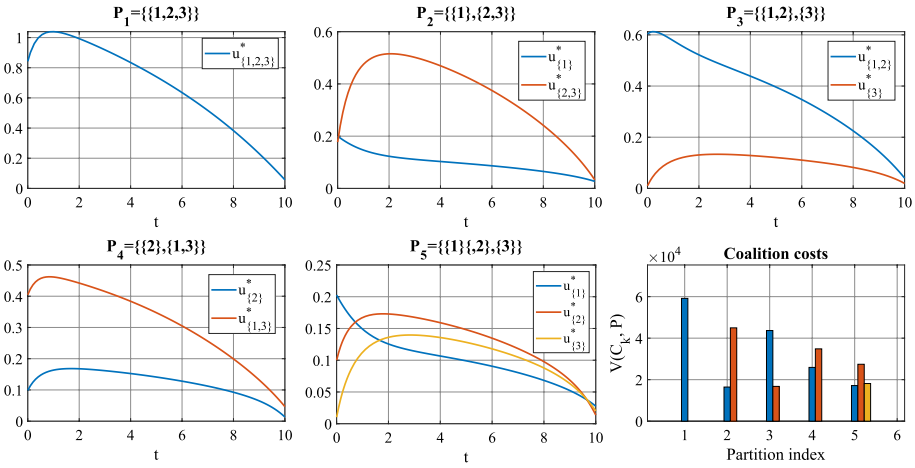

Fig. 5 Aggregated control trajectories $u^*_{\mathcal{C}_k}(t)$ for each partition: $P_1 = \{\{1,2,3\}\}$, $P_2 = \{\{1\},\{2,3\}\}$, $P_3 = \{\{1,2\},\{3\}\}$, $P_4 = \{\{2\},\{1,3\}\}$, $P_5 = \{\{1\},\{2\},\{3\}\}$. The bottom-right panel shows the bar chart of aggregated coalition costs $\mathcal{V}(\mathcal{C}_k, \mathcal{P}_i)$ for each partition

where the off-diagonal elements represent symmetric diffusion rates. The initial population densities are set to $x_1(0) = 600$, $x_2(0) = 100$, and $x_3(0) = 10$, indicating an advanced invasion in the protected area and early-stage infestations in the other regions. All other parameters follow the baseline configuration described in Table 1.

Figure 5 illustrates the aggregated optimal control trajectories $u^*_{\mathcal{C}_k}(t)$ associated with each coalition $\mathcal{C}_k$ across the five possible partitions $\mathcal{P}_i$ of the three-agent system. In each panel, the curves represent the collective control efforts exerted by each coalition, computed by summing the individual controls of its members. The bottom-right panel shows the total costs $\mathcal{V}(\mathcal{C}_k, \mathcal{P}_i)$ accrued by each coalition under the corresponding partition.

The aggregated control trajectories exhibit distinct temporal patterns depending on the coalition structure. In the fully cooperative partition $\mathcal{P}_1 = \{\{1,2,3\}\}$, the control effort initially rises sharply to counteract the high initial invasion, particularly in Area 1, and then gradually declines as population densities decrease. The resulting trajectory is smooth and sustained over the planning horizon, reflecting the system-wide optimization of efforts. For the partitions involving two coalitions ($\mathcal{P}_2$, $\mathcal{P}_3$, and $\mathcal{P}_4$), we observe differentiated control profiles across coalitions. Coalitions managing areas with higher habitat suitability or higher

Table 3 Comparison of Nash bargaining and Myerson allocations, relative to the cooperative total cost $J^{\mathrm{C}} = 59161.11$ €/km^2

Area	Competitive cost (€ /km^2)	Nash allocation (€/km^2)	Myerson allocation (€/km^2)
1	17146.36	15962.68	16434.75
2	27421.97	26238.30	25821.13
3	18143.81	16960.13	16905.22
Total	62712.14	59161.11	59161.11

initial infestation (e.g., coalitions containing Area 1) apply stronger and earlier control, whereas coalitions in less affected areas adopt weaker or delayed responses. This behavior highlights how strategic incentives differ when cooperation is limited to subgroups. In the fully non-cooperative case $\mathcal{P}_5 = \{\{1\}, \{2\}, \{3\}\}$, where each agent acts independently, the control trajectories are overall weaker and less synchronized compared to the cooperative case. Agents optimize their local objectives without accounting for cross-area externalities, leading to fragmented and suboptimal interventions. The cost bar plot confirms these observations: full cooperation ($\mathcal{P}_1$) minimizes the aggregate control cost, while partitions involving partial cooperation ($\mathcal{P}_2$, $\mathcal{P}_3$, $\mathcal{P}_4$) incur higher total costs. The non-cooperative outcome ($\mathcal{P}_5$) results in the highest overall cost, emphasizing the inefficiency of decentralized control in the presence of spatial externalities.

Table 3 compares the competitive costs and the cooperative allocations obtained under the Nash bargaining and Myerson allocation rules. In the Nash bargaining solution, an equal weighting scheme was adopted, assigning to each agent a bargaining power $\alpha_i = \frac{1}{3}$. The results highlight the benefits of cooperation among the three areas. In the non-cooperative setting, each agent incurs a higher control cost compared to the cooperative allocations, both under Nash bargaining and Myerson allocation rules. Specifically, Area 2 (the agricultural zone) faces the highest competitive cost, reflecting its greater vulnerability to invasive species damages, while Area 1 (the natural reserve) and Area 3 (the peri-urban area) experience lower (but still significant) competitive burdens.

Under cooperative agreements, the total cost substantially reduces from 62712.14 to 59161.11 €/km^2. In individual terms, all the areas achieve cost savings through cooperation. These reductions confirm that full cooperation is individually rational for all agents: each area achieves a strictly lower cost compared to acting independently. Further, this ensures that the cooperative outcome is *core-stable*, in the sense that no agent has an incentive to deviate (see Osborne and Rubinstein (1994)).

To facilitate a better reading of the results obtained, it is important to note that all costs reported in Table 3 are expressed per unit area (€/km^2). Therefore, the actual cost paid by each agent would also depend on the physical size of the managed area. Larger areas would naturally incur proportionally higher total expenditures even under uniform per-square-kilometer cost allocations.

Comparing the two allocation rules, slight differences emerge: the Myerson allocation grants a larger relative saving to Area 2, acknowledging its crucial role in mitigating spatial externalities, while slightly increasing the burden on Area 1 compared to the Nash outcome. This reflects the more refined treatment of strategic externalities under the Myerson value, as opposed to the simpler surplus allocation implied by Nash bargaining.

As discussed in Remark 3, the Myerson allocation implicitly determines a set of endogenous bargaining weights α_i^M, which quantify each agent's contribution to the cooperative surplus based on their marginal impact. In this case study, these weights are approximately

$\alpha_1^M \approx 0.20$, $\alpha_2^M \approx 0.45$, and $\alpha_3^M \approx 0.35$, respectively for Areas 1, 2, and 3. The interpretation is consistent with the observed cost dynamics: Area 2, which faces the highest non-cooperative burden and offers the greatest potential for cost reduction through cooperation, is assigned the highest bargaining power. Conversely, Area 1 receives the smallest weight, reflecting its poor marginal impact in the cooperative setting. These weights offer a principled rationale for the asymmetric allocation yielded by the Myerson value, reinforcing the ability of this approach in capturing network externalities–features that the Nash bargaining solution, with its fixed exogenous weights, fails to account for.

7 Conclusions and future perspectives

This work introduces a general dynamic framework for the management of invasive alien species in spatially structured settings, where multiple autonomous agents operate within their own areas of competence across a network of ecologically connected regions. Each agent is responsible for controlling the invasion locally, but spatial diffusion processes and ecological interdependencies shape the overall dynamics. In this setting, the model flexibly captures not only fully cooperative or purely non-cooperative behaviors, but also intermediate configurations in which subsets of agents form coalitions. Each coalition coordinates internal decisions to minimize the aggregate cost of its members, while interacting strategically with other coalitions across the network. This structure allows for the analysis of partial cooperation, reflecting real-world situations where institutional fragmentation or diverging interests prevent system-wide coordination.

In cooperative control scenarios, the allocation of total costs among agents is addressed through two complementary approaches. The Nash bargaining solution distributes the cooperative surplus according to fixed bargaining weights, reflecting predefined notions of fairness or negotiating power. The Myerson value, instead, derives each agent's share from their marginal contribution across all possible coalition structures, taking into account spatial externalities and the structure of ecological interactions. The comparison reveals that, while both approaches ensure individual rationality, the Myerson value leads to allocations that more accurately reflect the agents' ecological influence and strategic relevance within the network. Moreover, these allocations coincide with a Nash bargaining solution when bargaining weights are chosen consistently with the agents' marginal contributions to the cooperative surplus.

Our results clearly show that decentralized, competitive management tends to lead to suboptimal outcomes: overall invasion levels remain higher, control efforts are inconsistently applied, and aggregate costs to the system increase significantly. In contrast, full cooperation among agents enables more effective allocation of control efforts across space and time, leading to lower final population levels and substantially reduced economic costs. However, the simulations also reveal that cooperative agreements are inherently fragile. Even a single agent defecting from the cooperative strategy can erode the benefits for all participants and exacerbate invasion risks across the network. This finding underscores a critical policy implication: the sustainability of cooperative management arrangements depends not only on technical optimization but also on the design of an appropriate cost allocation that deters strategic defections or free-riding behaviors.

A natural extension of the model considers scenarios in which each agent manages multiple areas, enabling coordinated control efforts across several spatial subdomains. While each area remains distinct, the agent's strategy can be seen as a form of internal coordination, similar to a coalition structure, aimed at minimizing the collective cost of control efforts. This formulation preserves the key elements of spatial coupling and decentralized decision-making, while broadening the coalition framework to encompass agents responsible for multiple interconnected regions. A relevant application arises in lattice-based grids, where each agent controls a subset of discrete spatial units (e.g., cells), as in Büyüktahtakin et al. (2011). In this case, the diffusion matrix S corresponds to the finite-difference discretization of the Laplacian operator used in reaction–diffusion models (see, e.g., Baker et al. (2018)). This connection opens the door to hybrid models that integrate PDE-based spatial ecology with discrete multi-agent control, and will be explored further, including feedback-based and adaptive strategies.

While the present model offers valuable insights into the management of invasive species across spatial networks, several opportunities for extensions remain, which could enhance the model's ecological realism, computational tractability, and relevance for real-world decision-making processes. From a modeling perspective, this work assumed symmetric diffusion coefficients, reflecting undirected and reciprocal motion between areas. This formulation ensures a conservative redistribution, suitable for scenarios where species dispersal is not influenced by directional forces. The diffusion was modeled as linear and proportional to population size differences, capturing typical spread patterns from high- to low-density regions. Future extensions could incorporate asymmetric or state-dependent diffusion processes to account for environmental heterogeneity, preferential movement paths (e.g., ecological corridors), and directional transport phenomena, such as wind or water currents (Marangi et al., 2023). Additionally, movement driven by external stimuli, such as chemotaxis, could be integrated (Monti et al., 2025).

From a computational perspective, while the model provides a general framework for both open-loop and state-feedback strategies, numerical challenges arise for large N in both formulations. In particular, solving the Hamilton–Jacobi–Bellman equation for feedback strategies becomes computationally demanding. To address this, we plan to employ model order reduction techniques (Schilders et al., 2008) to efficiently approximate feedback equilibria, preserving key system dynamics. Additionally, adaptive methodologies, both physics-based (Alla et al., 2023) and data-driven (Alla et al., 2024), will be explored to enhance computational efficiency by adapting to evolving system features.

Appendix A: Technical proofs

Proof of Proposition 2 First, observe that the state system (4) is well-posed for all u, due to the regularity of the functions $f_i(x_i)$ and $g_i(x_i)$ (Assumption (A1)), and the linearity of the diffusion operator. This ensures the existence and uniqueness of a local solution $\mathrm{x}(t)$. The growth condition in Assumption (A2) provides a global bound on the right-hand side, which guarantees that the solution can be extended to the entire interval $[0, T]$, and ensures the continuous dependence of $\mathrm{x}(t)$ on the initial state x_0 and on the control function $\mathrm{u}(t)$.

The positivity of the solution follows from Assumption (A3). Suppose that, at some time t, we have $x_i(t) = 0$ for some i. Then, using $f_i(0) = g_i(0) = 0$, the dynamics reduce to:

$$\dot{x}_i(t) = \sum_{j=1}^{N} \sigma_{ij} x_j(t) \geq 0.$$

This implies that $x_i(t)$ cannot decrease below zero. Hence, the non-negative orthant is forward invariant, and no trajectory starting from $x_i(0) \geq 0$ can become negative. □

Proof of Proposition 3 The result follows by adapting the standard direct method in the calculus of variations, as applied in Di Liddo and Martiradonna (2025), where existence of optimal controls is established for a related single-agent model.

For each agent $i = 1, \ldots, N$, fix the strategies $\mathrm{u}_{-i} \in \mathcal{U}^{N-1}$ of the other agents. Under Assumptions (A1)–(A4), the cost functional $J_i(u_i, \mathrm{u}_{-i})$ is non-negative and weakly lower semicontinuous in $L^2(0,T)$, and the state system is well-posed with trajectories depending continuously on the control inputs (cf. Proposition 2).

Therefore, a minimizing sequence admits a weakly convergent subsequence whose limit is admissible and achieves the infimum, yielding an optimal response $u_i^* \in \mathcal{U}$. Repeating the argument for each agent yields a profile $\mathrm{u}^* \in \mathcal{U}^N$ such that no agent has an incentive to deviate unilaterally, hence u^* is a Nash equilibrium for game (6). □

Proof of Proposition 4 We apply Pontryagin's Maximum Principle to the individual optimization problem of each agent i, treating the strategies u^*_{-i} of the other agents as fixed. The individual Hamiltonian of agent i, used in the following derivations, is defined in Eq. 8).

Then, for each agent i, there exists an absolutely continuous vector of adjoint variables

$$\boldsymbol{\lambda}_i^\top(t) = (\lambda_{i1}(t), \lambda_{i2}(t), \ldots, \lambda_{iN}(t))$$

such that the following necessary conditions hold almost everywhere on $[0,T]$:

$$\begin{aligned}
\dot{\mathrm{x}}^*(t) &= \mathrm{f}(\mathrm{x}^*(t)) + S\,\mathrm{x}^*(t) - G(\mathrm{x}^*(t))\,\mathrm{u}^*(t), \quad \mathrm{x}^*(0) = \mathrm{x}_0,\\
\dot{\boldsymbol{\lambda}}_i(t) &= \rho\,\boldsymbol{\lambda}_i(t) - \nabla_{\mathrm{x}} \mathcal{H}_i(\mathrm{x}^*(t), \boldsymbol{\lambda}_i(t), u^*(t)), \quad \text{for all } i = 1, \ldots, N,\\
u_i^*(t) &= \arg\min_{u_i \in \mathcal{U}} \mathcal{H}_i(\mathrm{x}^*(t), \boldsymbol{\lambda}_i(t), u_i, \mathrm{u}^*_{-i}), \quad \text{for all } i = 1, \ldots, N,\\
\boldsymbol{\lambda}_i(T) &= \nabla_{\mathrm{x}} \phi_i(x_i^*(T)), \quad \text{for all } i = 1, \ldots, N.
\end{aligned}$$

We collect all the adjoint vectors $\boldsymbol{\lambda}_i^\top(t)$ into the matrix

$$\Lambda(t) = \begin{bmatrix} \boldsymbol{\lambda}_1^\top(t) \\ \boldsymbol{\lambda}_2^\top(t) \\ \vdots \\ \boldsymbol{\lambda}_N^\top(t) \end{bmatrix} \in \mathbb{R}^{N \times N}.$$

To derive the explicit form of the adjoint equation, we compute the components of the gradient $\nabla_{\mathrm{x}} \mathcal{H}_i$ as follows:

$$\frac{\partial \mathcal{H}_i}{\partial x_j} = \delta_{ij} E_i'(x_i) + \sum_{k=1}^{N} \lambda_{ik} \left(\delta_{jk} \left[f_k'(x_k) - g_k'(x_k) u_k \right] + S_{kj} \right)$$

$$= \delta_{ij} E_i'(x_i) + \lambda_{ij} \left(f_j'(x_j) - g_j'(x_j)\, u_j \right) + \sum_{k=1}^{N} \lambda_{ik} S_{kj}.$$

Using the identity $S_{kj} = \sigma_{kj} - \delta_{jk} \sum_{\ell=1}^{N} \sigma_{k\ell}$, we obtain:

$$\sum_{k=1}^{N} \lambda_{ik} S_{kj} = \sum_{k=1}^{N} \sigma_{jk} (\lambda_{ij} - \lambda_{ik}),$$

and therefore:

$$\frac{\partial \mathcal{H}_i}{\partial x_j} = \delta_{ij} E_i'(x_i) + \lambda_{ij} \left(f_j'(x_j) - g_j'(x_j)\, u_j \right) + \sum_{k=1}^{N} \sigma_{jk} (\lambda_{ij} - \lambda_{ik}).$$

The transversality condition for each λ_{ij} is:

$$\lambda_{ij}(T) = \delta_{ij} \phi_i'(x_i(T)).$$

Finally, the minimization of the Hamiltonian in u_i yields:

$$0 = \frac{\partial \mathcal{H}_i}{\partial u_i} = d_i u_i - \lambda_{ii} g_i(x_i),$$

which gives the optimal control in feedback form:

$$u_i = \frac{1}{d_i} \lambda_{ii} g_i(x_i).$$

Finally, given the non-negativity constraint $u_i(t) \geq 0$ and to account for possible boundary solutions, the optimal control takes the form:

$$u_i^*(t) = \max \left\{ 0,\ \frac{1}{d_i} \lambda_{ii}(t)\, g_i(x_i^*(t)) \right\}.$$

□

Proof of Proposition 7 The objective function in (15) is strictly concave, and the feasible set is convex. Standard results guarantee the existence and uniqueness of the optimal solution. To compute it explicitly, we apply the method of Lagrange multipliers. Taking the logarithm of the objective (which preserves monotonicity), we obtain the equivalent problem:

$$\max_{0\le c_i<J_i^{\mathrm{NC}}} \sum_{i=1}^{N} \alpha_i \log\left(J_i^{\mathrm{NC}} - c_i\right) \quad \text{subject to} \quad \sum_{i=1}^{N} c_i = J^{\mathrm{C}}.$$

We introduce the Lagrangian:

$$\mathcal{L}(\mathrm{c},\lambda) = \sum_{i=1}^{N} \alpha_i \log\left(J_i^{\mathrm{NC}} - c_i\right) + \lambda\left(\sum_{i=1}^{N} c_i - J^{\mathrm{C}}\right).$$

The first-order condition with respect to each c_i yields:

$$\frac{\partial \mathcal{L}}{\partial c_i} = -\frac{\alpha_i}{J_i^{\mathrm{NC}} - c_i} + \lambda = 0 \quad \Rightarrow \quad c_i = J_i^{\mathrm{NC}} - \frac{\alpha_i}{\lambda}.$$

Substituting into the constraint $\sum_{i=1}^{N} c_i = J^{\mathrm{C}}$, we obtain:

$$\sum_{i=1}^{N}\left(J_i^{\mathrm{NC}} - \frac{\alpha_i}{\lambda}\right) = J^{\mathrm{C}} \quad \Rightarrow \quad \sum_{i=1}^{N} J_i^{\mathrm{NC}} - \frac{1}{\lambda} = J^{\mathrm{C}} \quad \Rightarrow \quad \lambda = \frac{1}{\sum_{i=1}^{N} J_i^{\mathrm{NC}} - J^{\mathrm{C}}}.$$

Substituting this into the expression for c_i yields:

$$c_i^* = J_i^{\mathrm{NC}} - \alpha_i\left(\sum_{j=1}^{N} J_j^{\mathrm{NC}} - J^{\mathrm{C}}\right),$$

which completes the proof. □

Proof of Proposition 8 Starting from (18), summing over all players i, we have

$$\sum_{i=1}^{N} \psi_i(\mathcal{V}) = \mathcal{V}(\mathcal{N},\{\mathcal{N}\}) + \sum_{(\mathcal{C},\mathcal{P})\neq(\mathcal{N},\{\mathcal{N}\})} (-1)^{|\mathcal{P}|-1}\,(|\mathcal{P}|-1)!\left(\sum_{i=1}^{N}\left(\frac{1}{N} - \omega_i(\mathcal{C},\mathcal{P})\right)\right)\mathcal{V}(\mathcal{C},\mathcal{P}).$$

Observe that

$$\sum_{i=1}^{N}\left(\frac{1}{N} - \omega_i(\mathcal{C},\mathcal{P})\right) = 1 - \sum_{i=1}^{N}\omega_i(\mathcal{C},\mathcal{P}).$$

We now show that for any $(\mathcal{C},\mathcal{P}) \neq (\mathcal{N},\{\mathcal{N}\})$,

$$\sum_{i=1}^{N}\omega_i(\mathcal{C},\mathcal{P}) = 1.$$

Indeed, by the definition of ω_i,

$$\sum_{i\in\mathcal{N}} \omega_i(\mathcal{C},\mathcal{P}) = \sum_{\substack{\mathcal{D}\in\mathcal{P}\\ \mathcal{D}\neq\mathcal{C}}} \sum_{\substack{i\in\mathcal{N}\\ i\notin\mathcal{D}}} \frac{1}{(|\mathcal{P}|-1)(N-|\mathcal{D}|)}.$$

For each fixed $\mathcal{D}\neq\mathcal{C}$, there are exactly $N-|\mathcal{D}|$ players not in $\mathcal{D}$, each contributing the same amount. Thus,

$$\sum_{\substack{i\in\mathcal{N}\\ i\notin\mathcal{D}}} \frac{1}{(|\mathcal{P}|-1)(N-|\mathcal{D}|)} = \frac{1}{|\mathcal{P}|-1}.$$

Summing over the $|\mathcal{P}|-1$ coalitions different from $\mathcal{C}$ gives

$$\sum_{i=1}^{N} \omega_i(\mathcal{C},\mathcal{P}) = (|\mathcal{P}|-1)\frac{1}{|\mathcal{P}|-1} = 1.$$

Therefore, $1-\sum_{i=1}^{N}\omega_i(\mathcal{C},\mathcal{P})=0$ for all $(\mathcal{C},\mathcal{P})\neq(\mathcal{N},\{\mathcal{N}\})$, and we conclude that

$$\sum_{i=1}^{N}\psi_i(\mathcal{V}) = \mathcal{V}(\mathcal{N},\{\mathcal{N}\}),$$

as claimed. □

Supplementary Information The online version contains supplementary material available at https://doi.org/10.1007/s10479-025-06759-6.

Acknowledgements The authors are members of Gruppo Nazionale per l'Analisi Matematica, la Probabilità e le loro Applicazioni - Istituto Nazionale di Alta Matematica (GNAMPA-INdAM). A.M. acknowledges fruitful discussions with Sabrina Francesca Pellegrino following her presentation at the Second Workshop on Mathematical Challenges in Ecology and Biology (Politecnico di Bari), which provided inspiration for the multi-area extension of the model. We thank the two anonymous reviewers for their careful reading and helpful remarks.

Author contributions All authors contributed equally to this work.

Funding Open access funding provided by Università di Foggia within the CRUI-CARE Agreement. A.D.L and A.M. have been supported by the PRA 2024 project "Strategic Interactions in Economics, Ecology and Health", funded by Università di Foggia.

Data availability No data were used in this work.

Code availability Codes are available on request.

Declarations

Conflict of interest The authors declare that they have no conflict of interest.

Ethical approval Not applicable.

Consent for publication Not applicable.

References

Ahmed, D. A., Hudgins, E. J., Cuthbert, R. N., Kourantidou, M., Diagne, C., Haubrock, P. J., Leung, B., Liu, C., Leroy, B., Petrovskii, S., et al. (2022). Managing biological invasions: The cost of inaction. *Biological Invasions, 24*(7), 1927–1946.

Alla, A., Monti, A., & Sgura, I. (2023). Adaptive POD-DEIM correction for Turing pattern approximation in reaction–diffusion pde systems. *Journal of Numerical Mathematics, 31*(3), 205–229.

Alla, A., Monti, A., & Sgura, I. (2024). Piecewise DMD for oscillatory and Turing spatio-temporal dynamics. *Computers & Mathematics with Applications, 160*, 108–124.

Baker, C. M., Blonda, P., Casella, F., Diele, F., Marangi, C., Martiradonna, A., Montomoli, F., Pepper, N., Tamborrino, C., & Tarantino, C. (2023). Using remote sensing data within an optimal spatiotemporal model for invasive plant management: the case of Ailanthus altissima in the Alta Murgia National Park. *Scientific Reports, 13*(1), 14587.

Baker, C. M., Diele, F., Lacitignola, D., Marangi, C., & Martiradonna, A. (2019). Optimal control of invasive species through a dynamical systems approach. *Nonlinear Analysis: Real World Applications, 49*, 45–70.

Baker, C. M., Diele, F., Marangi, C., Martiradonna, A., & Ragni, S. (2018). Optimal spatiotemporal effort allocation for invasive species removal incorporating a removal handling time and budget. *Natural Resource Modeling, 31*(4), 12190.

Bertsekas, D. (2012). *Dynamic programming and optimal control* (Vol. I). Athena scientific.

Bischi, G. I., Lamantia, F., & Sbragia, L. (2009). Strategic interaction and imitation dynamics in patch differentiated exploitation of fisheries. *Ecological Complexity, 6*(3), 353–362.

Brown, P., & Daigneault, A. (2014). Cost-benefit analysis of managing the invasive African tulip tree (Spathodea campanulata) in the pacific. *Environmental science & policy, 39*, 65–76.

Büyüktahtakin, I.E., Feng, Z., Szidarovszky, F., & Frisvold, G. (2011). A game theoretical approach to invasive species management. In: IIE Annual Conference. Proceedings, p. 1. Institute of Industrial and Systems Engineers (IISE)

Chung, F. R. K. (1997). *Spectral graph theory* (Vol. 92). American Mathematical Society.

Cobourn, K. M., Amacher, G. S., & Haight, R. G. (2019). Cooperative management of invasive species: A dynamic nash bargaining approach. *Environmental and resource economics, 72*, 1041–1068.

Cuomo, S., Di Cola, V. S., Giampaolo, F., Rozza, G., Raissi, M., & Piccialli, F. (2022). Scientific machine learning through physics-informed neural networks: Where we are and what's next. *Journal of Scientific Computing, 92*(3), 88.

Di Liddo, A., & Martiradonna, A. (2025). Effective management of invasive alien species in an optimal control framework. Decisions in Economics and Finance, 1–32 https://doi.org/10.1007/s10203-025-00525-w

Epanchin-Niell, R. S., & Wilen, J. E. (2012). Optimal spatial control of biological invasions. *Journal of Environmental Economics and Management, 63*(2), 260–270.

Eppinga, M. B., Baudena, M., Haber, E. A., Rietkerk, M., Wassen, M. J., & Santos, M. J. (2021). Spatially explicit removal strategies increase the efficiency of invasive plant species control. *Ecological Applications, 31*(3), 02257.

Fabbri, G., Faggian, S., & Freni, G. (2024). Growth models with externalities on networks. Decisions in Economics and Finance, 1–22. https://doi.org/10.1007/s10203-024-00496-4

Falcone, M. (2006). Numerical methods for differential games based on partial differential equations. *International Game Theory Review, 8*(02), 231–272.

Fernandez, L. (2011). Economic incentives to prevent aquatic invasive species in wetlands. *Canadian Journal of Agricultural Economics/Revue canadienne d'agroeconomie, 59*(2), 281–293.
Hauser, C. E., & McCarthy, M. A. (2009). Streamlining 'search and destroy': Cost-effective surveillance for invasive species management. *Ecology Letters, 12*(7), 683–692.
Holling, C. S. (1959). Some characteristics of simple types of predation and parasitism1. *The Canadian entomologist, 91*(7), 385–398.
Kóczy, L. Á., et al. (2018). Partition function form games. *Theory and Decision Library C, 48*, 312.
Lampert, A., Hastings, A., Grosholz, E. D., Jardine, S. L., & Sanchirico, J. N. (2014). Optimal approaches for balancing invasive species eradication and endangered species management. *Science, 344*(6187), 1028–1031.
Mancinelli, G., Lago, N., Scirocco, T., Lillo, O. A., De Giorgi, R., Doria, L., Mancini, E., Mancini, F., Potenza, L., & Cilenti, L. (2024). Abundance, size structure, and growth of the invasive blue crab callinectes sapidus in the lesina lagoon, southern adriatic sea. *Biology, 13*(12), 1051.
Marangi, C., Casella, F., Diele, F., Lacitignola, D., Martiradonna, A., Provenzale, A., & Ragni, S. (2020). Mathematical tools for controlling invasive species in protected areas. Mathematical Approach to Climate Change and its Impacts: MAC2I, 211–237
Marangi, C., Martiradonna, A., & Ragni, S. (2023). Optimal resource allocation for spatiotemporal control of invasive species. *Applied Mathematics and Computation, 439*, 127614.
Martiradonna, A., Diele, F., & Marangi, C. (2020). Optimal control of invasive species with budget constraint: qualitative analysis and numerical approximation. Current Trends in Dynamical Systems in Biology and Natural Sciences, pp. 147–164
Mehta, S. V., Haight, R. G., Homans, F. R., Polasky, S., & Venette, R. C. (2007). Optimal detection and control strategies for invasive species management. *Ecological Economics, 61*(2–3), 237–245.
Monti, A., Diele, F., Lacitignola, D., & Marangi, C. (2025). Patterns in soil organic carbon dynamics: Integrating microbial activity, chemotaxis and data-driven approaches. *Mathematics and Computers in Simulation, 234*, 86–101.
Myerson, R. B. (1977). Graphs and cooperation in games. *Mathematics of Operations Research, 2*(3), 225–229.
Nash, J. F. (1950). The bargaining problem. *Econometrica, 18*(2), 155–162. https://doi.org/10.2307/1907266
Osborne, M. J., & Rubinstein, A. (1994). *A course in game theory*. MIT Press.
Pimentel, D., McNair, S., Janecka, J., Wightman, J., Simmonds, C., O'connell, C., Wong, E., Russel, L., Zern, J., Aquino, T., et al. (2001). Economic and environmental threats of alien plant, animal, and microbe invasions. *Agriculture, ecosystems & environment, 84*(1), 1–20.
Pontryagin, L. S. (2018). *Mathematical theory of optimal processes*. Routledge.
Scalera, R., Genovesi, P., Essl, F., & Rabitsch, W. (2012). The impacts of invasive alien species in europe. Technical report, European Environment Agency EEA Technical report No 16/2012
Schilders, W. H., Vorst, H. A., & Rommes, J. (2008). Model Order Reduction: Theory, Research Aspects and Applications vol. 13. Springer
Shapley, L. S. (1953). A value for n-person games. *Contributions to the Theory of Games, 2*(28), 307–317.
Siriwardena, S. D., Cobourn, K. M., Amacher, G. S., & Haight, R. G. (2018). Cooperative bargaining to manage invasive species in jurisdictions with public and private lands. *Journal of Forest Economics, 32*, 72–83.
Thrall, R. M., & Lucas, W. F. (1963). N-person games in partition function form. *Naval Research Logistics Quarterly, 10*, 281–298.
Warziniack, T., Haight, R. G., Yemshanov, D., Apriesnig, J. L., Holmes, T. P., Countryman, A. M., Rothlisberger, J. D., & Haberland, C. (2021). Economics of invasive species. Invasive Species in Forests and Rangelands of the United States: A Comprehensive Science Synthesis for the United States Forest Sector, 305–320
With, K. A. (2002). The landscape ecology of invasive spread. *Conservation Biology, 16*(5), 1192–1203. https://doi.org/10.1046/j.1523-1739.2002.01064.x